9 WATER INGRESS

This chapter is involved with the investigation of the effect of exposure to water on cured epoxy resin blocks of two of the previously studied systems (Prime20 and the shared model system). Blocks were prepared according to cure schedules described in Chapter 3. The cured blocks were cut to a size of 48 mm x 48 mm x 2 mm and immersed in deionised water. Dielectric spectroscopy was used to analyse the blocks, which were periodically removed from the water, and the results were then compared to those generated from gravimetric analysis. Prior to immersion, the glass transition temperature (T_g) of each of the samples was found by using differential scanning calorimetry (DSC). The DSC measurements were also performed to determine the extent of cure which had been achieved.

9.1 PREPARATION OF SAMPLES

The cure schedules and the preparation technique for the two systems studied in this chapter were discussed in *Chapter 3, Section 3.4.1*. Both Prime20 and the shared model system were cured at 50ºC, 60ºC and 70ºC. The large blocks were cut to the required size of 48 mm x 48 mm (± 2 mm error in measurement), and there were three blocks of each sample produced. The water ingress was studied at two aging temperatures, 50ºC and 70ºC, as agreed with the other ACLAIM collaborators. Prior to analysis, the average thickness of each sample block was found by measuring the thickness at each corner and also in the centre of the block. The overall thickness for each of the two systems is as follows, where the error is the standard deviation:

Prime20:	1.99 ± 0.02 mm
Shared Model System:	1.98 ± 0.03 mm

The thickness of the samples used for the diffusion measurements was sufficiently small relative to the area that the diffusion through the edges can be neglected relative to that through the faces. The area of the edges is *ca.* 384 mm^2 compared with *ca.* 4608 mm^2, which implies *ca.* 8% of the water uptake is through the edges.

This is not negligible but is sufficiently small to allow the planar diffusion models to be applied to the data.

In principle, the T_g is a controlling factor in determining the diffusion of low molar mass species into a polymeric solid and therefore is an important parameter which should be determined for each sample. Likewise, the presence of uncured monomer can potentially plasticise the matrix and enhance the rate of diffusion. Therefore knowledge of both the T_g and the extent of cure is important if correlations between diffusion behaviour and molecular structure are to be attempted.

9.2 DSC OF CURED BLOCKS

As previously discussed (*Chapter 3, Section 3.4.1*) the cured sample blocks were analysed by DSC on a heat-cool-reheat cycle to assess the T_g of the samples at each cure temperature. Each system had been cured at three different temperatures according to the agreed cure schedule, and samples from each of these were repeated three times to allow an average T_g to be calculated, along with an error in the value. Comparison of the first heat scan with the second (reheat) scan gives an indication of the residual cure in the samples that would be immersed in water.

9.2.1 Prime20

An example of the heat-cool-reheat scan is shown in Figure 1 for a Prime20 block cured at 50ºC. Taking the repeat1 set of scans (the black lines in the figure below), reading up the heat flow axis from approximately 75ºC on the x-axis, the first line is the heat scan, the top line is the cool scan and the middle one is the reheat scan. The scans for blocks cured at 60ºC and 70ºC can be found in the appendices.

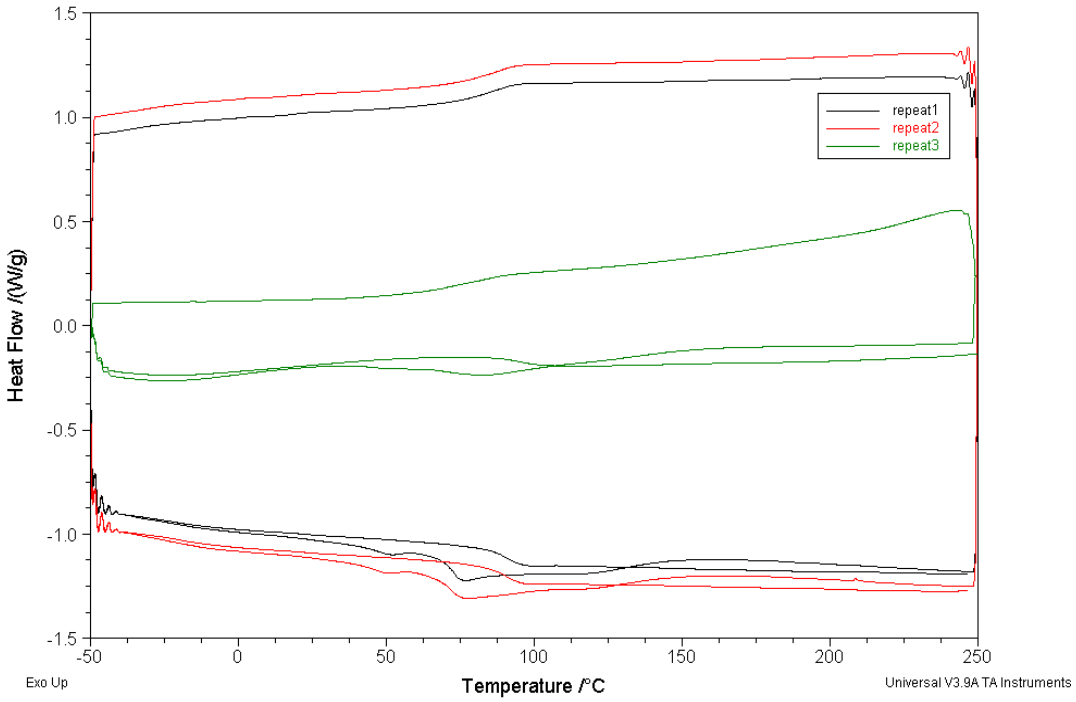

Figure 1. DSC scans of Prime20 system cured at 50ºC showing heat flow vs. temperature.

Repeat3 was done later than the first two repeats after the DSC head had suffered some damage (which was not remedied within the time of this study). This lead to a more pronounced sloping baseline, and the introduction of an apparent exothermic peak prior to the T_g on both the initial heating scan and the reheat scan, as can be clearly seen in Figure 1 and also the figures contained in the appendices. While these introduce a bigger error into the T_g estimation, the repeat3 T_g values for each step of the cycle are not vastly different compared to repeat1 and repeat2 and so the data has been included in the calculation of an average value for the T_g.

Figure 2 shows an overlay for the blocks cured at 50ºC; 60ºC and 70ºC, and allows a comparison of the three blocks to be made more easily. In the initial heating scan, a broad exothermic peak can be observed after the T_g, and this is due to residual cure, i.e. this event is evident as further crosslinking occurs. A slight dip may be observed prior to the T_g in the initial heating scan in all three samples, although it is less pronounced in the block cured at 70ºC. This event can be seen in all of the scans, including the repeat3 scans, albeit it is more difficult to observe due to the 'exothermic' peak prior to the T_g.

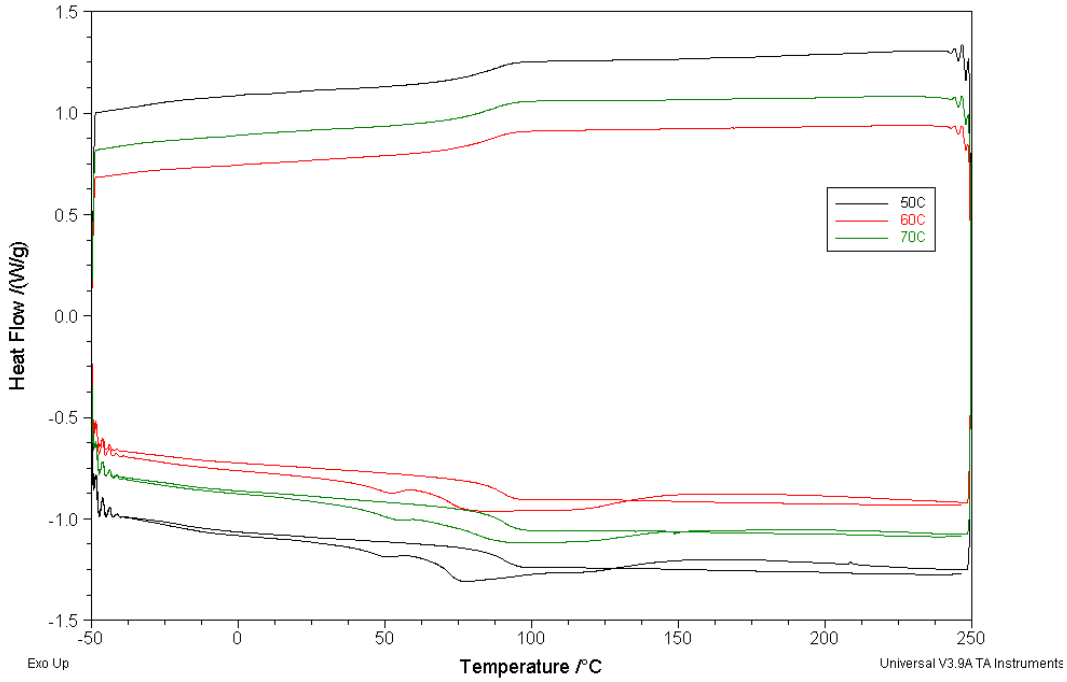

Figure 2. Overlay of DSC scans for Prime20 system cured at 50°C (-), 60°C(-) and 70°C(-) showing heat flow vs. temperature.

This dip could be the result of a network relaxation - as the cure proceeds the T_g increases and the chain mobility decreases causing the potential for chains to be locked in out-of-equilibrium conformations. As energy is added to the (cured) system the chains are able to move to their preferred conformation and so a relaxation is observed [1, 2]. A shift of the T_g on post cure of the sample is often observed in thermoset materials where stresses are created in the matrix as a consequence of the T_g processes suppressing the ability of the chain backbone motion to equilibrate the conformations of the matrix as it is formed. Another explanation of the shift in T_g could be that there is a little unreacted material present that has not been fully incorporated into the network and so there are two phases - leading to two glass transition steps. Presented work on the cure of cross-linked vinyl polymers [3], where a crosslinker was incorporated into a free radical polymerisation, has shown a similar effect with two distinct T_g's due to two phases.

One way to investigate the event further would be to utilise solid state proton nuclear magnetic resonance (NMR) where a lower molecular weight material would have more mobile protons compared to the quite immobile network protons and so a two phase system could be potentially observed. This was not carried out as the cure

schedules were agreed with the project consortium and could not be easily altered, and so it was felt that any further investigation was outwith the remit of this study.

The T_g was calculated for each of the heat, cool, reheat scans and the average (of the three repeats) is plotted in Figure 3, where the standard deviation of the repeats was used for the error bars.

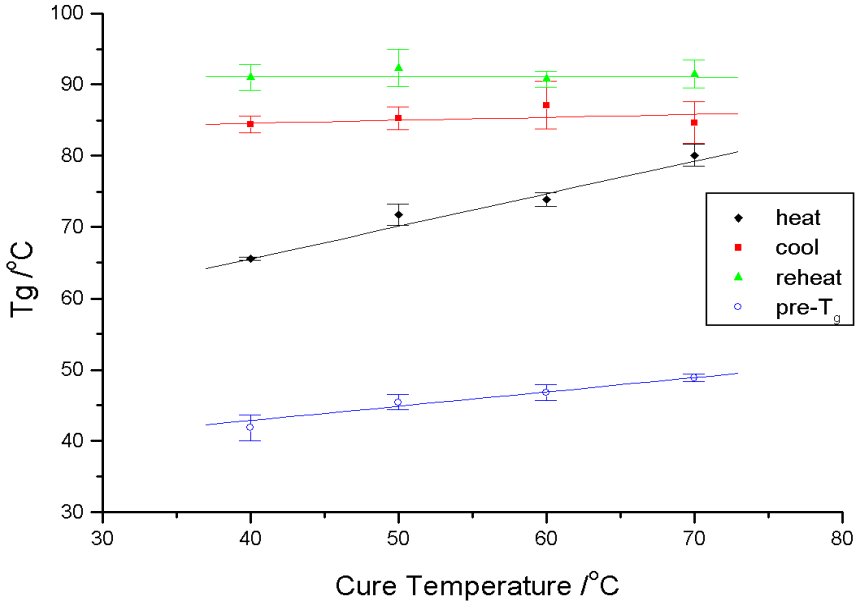

Figure 3. Glass transition temperatures from DSC heat, cool and re-heat scans of cured Prime20 blocks, as a function of the cure temperature.

The heat scan T_g increases with increasing cure temperature, from 72ºC (50ºC cure) to 80ºC (70ºC). The cool and reheat T_g remains constant as the cure temperature is increased - 86ºC (cool) and 92ºC (reheat). This behaviour is expected as on the initial heating scan the samples were taken well above their cure temperature allowing any further reaction to occur before the cooling scan. An increase in the value of T_g with increasing cure temperature is commonly observed for thermoset network systems and is consistent with the concepts discussed previously with regards the TTT diagrams for such systems. The cool values are higher than those for the reheat due to hysteresis effects. The dip seen prior to the initial heat T_g also shows a slight increase on increasing cure temperature: 45ºC (50ºC cure) to 49ºC (70ºC cure). This increase would tend to imply it is due to a second phase as opposed to a relaxation, where it would be expected to remain linear.

To verify these results a block was cured at 40ºC and analysed in the same way. This gave an initial heat T_g of 66ºC which falls on the slope shown in Figure 3. The cool and reheat values remained constant. The value for the pre-T_g event was 42ºC which verifies that the value increases linearly as the cure temperature is increased.

The area under the broad exothermic peak seen after the T_g, taken from the initiation of the peak until 200°C and integrated linearly, decreases with increasing cure temperature for the heat scan and remains closer to zero for the reheat as expected. On the reheat there is residual entropy frozen into the system due to the cooling rate used on the cool scan, resulting in values that are not zero. Due to the differences between the first two and last repeat, only the first two repeats for Prime20 have been used in the calculation of residual cure, where the average difference between the heat and reheat values was divided by the average value of the dynamic scans found in Chapter 5 (476.7 J/g). The results are shown in Table 1. It should be noted that for the blocks cured at 60°C there was a dip in the scans within the range integrated resulting in a lower heat, but higher reheat value giving a lower than anticipated residual cure value.

Table 1. Heat, reheat and residual cure values for Prime20 blocks.

T_c /°C	Scan	Heat (J/g)	Reheat (J/g)	Average Residual Cure*
40	repeat1	15.98	1.326	**3.2%**
	repeat2	14.34	0.4467	
	repeat3	7.709	0.6442	
50	repeat1	12.86	0.1649	**2.6%**
	repeat2	11.5	0.4992	
	repeat3	7.135	0.1737	
60	repeat1	1.721	7.54	**1.5%**
	repeat2	12.67	0.2962	
	repeat3	8.316	0.534	
70	repeat1	9.777	0.2755	**1.8%**
	repeat2	7.429	0.4275	
	repeat3	5.544	0.2643	

* using repeat1 and repeat2 only

9.2.2 Shared Model System

All of the scans for the shared model system were carried out after the damage to the DSC head was inflicted and show the same sloping baseline and 'exothermic' peak that the repeat3 scans did for the previous system. This reinforces the idea that the apparent exotherm is associated with the instrument and not the sample. Figure 4 shows the three repeat scans from the block cured at 50ºC, with the plots for those cured at 60ºC and 70ºC in the appendices.

Figure 5 shows the overlay of the second repeat scans for the blocks cured at 50ºC 60ºC and 70ºC, and allows a comparison of the three blocks to be made more easily. As previously shown, a slight dip may be observed prior to the T_g in the initial heating scan in all three samples, although it is less pronounced in the block cured at 70ºC. This event can be seen in all of the scans, including the repeat3 scans, albeit it is more difficult to observe due to the exothermic peak, which as expected decreases (area under the curve) with increasing cure temperature.

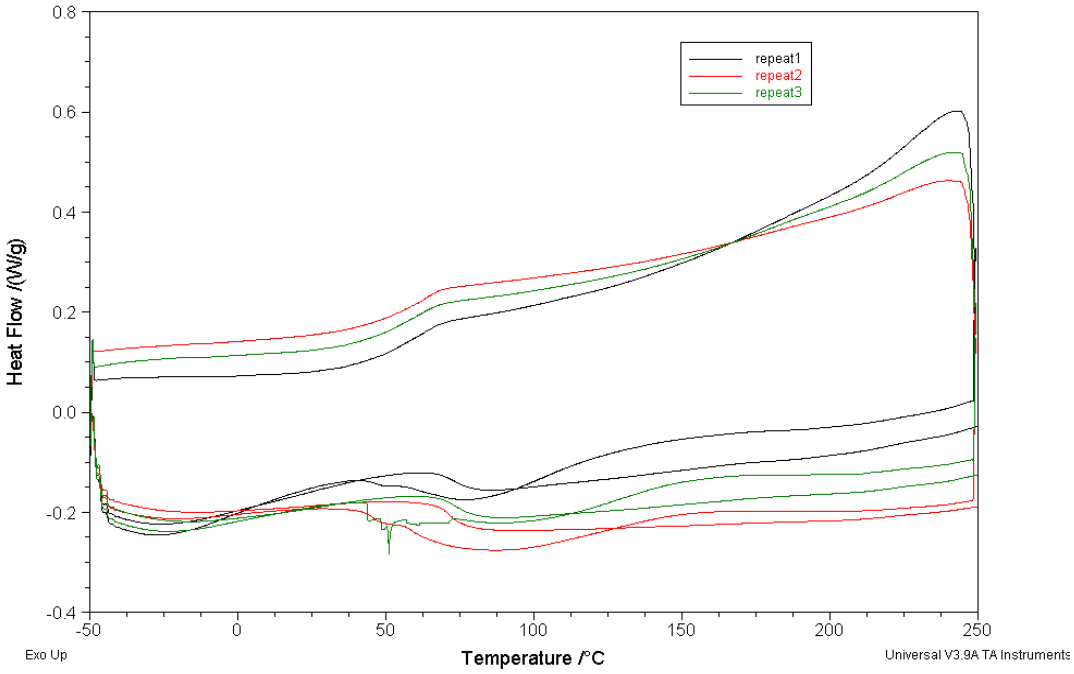

Figure 4. DSC scans of Shared Model system cured at 50ºC showing heat flow vs. temperature.

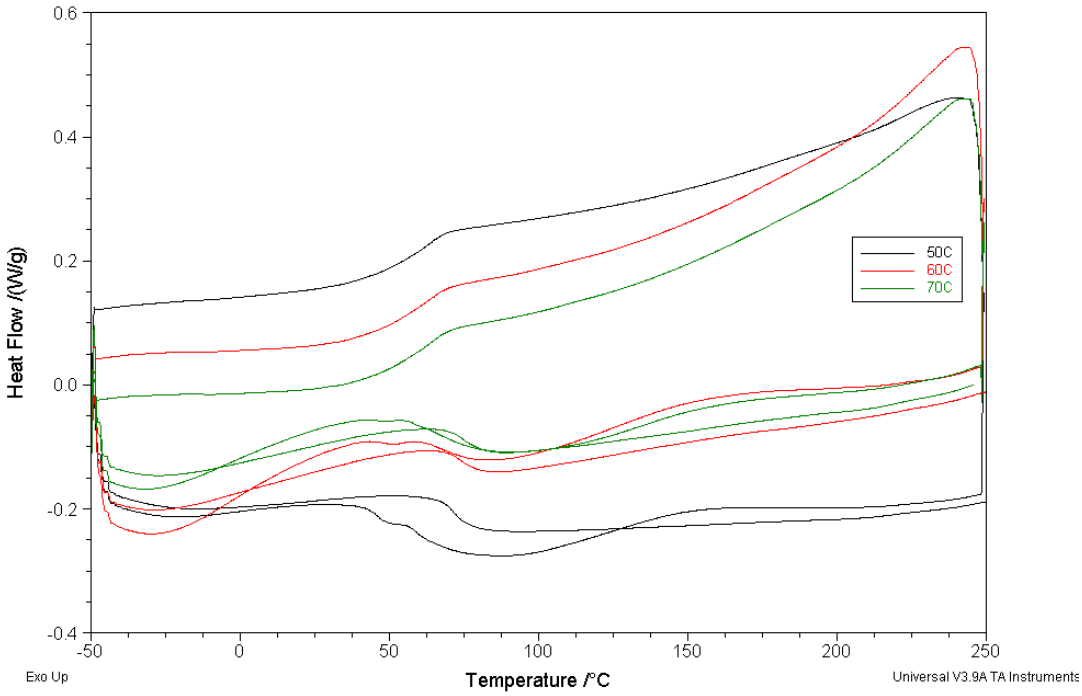

Figure 5. Overlay of DSC scans for shared model system cured at 50ºC (-), 60ºC(-) and 70ºC(-) showing heat flow vs. temperature.

The T_g was calculated for each of the heat, cool, reheat scans and the average (of the three repeats) is plotted in Figure 6. The heat scan T_g increases with increasing cure temperature from 60ºC for the block cured at 50ºC to 66ºC for the 60ºCcured block, and remains constant (within error bars) for the block cured at 70ºC. The cool T_g increases slightly from 63ºC to 65ºC, which is lower than the heat value for the blocks cured at 60ºC and 70ºC, and the linear line crosses through the heat data. It was thought that due to the problems the instrument was experiencing at the time of the analysis the cooling rate of 10ºC min $^{-1}$ might not have been achieved. However, when the data table for each sample was checked, the cooling rate was as expected. This unexpected phenomenon was not investigated as the cure schedules had been set as previously explained. The reheat values appear to increase slightly from 73ºC (50ºC) to 75ºC (70ºC). When the error bars are considered for the cool and reheat results, a straight line could just be drawn through each of the three points. The dip seen prior to the initial heat T_g appears to remain constant at 47ºC upon increasing cure temperature. However the error bar for the 50ºC cure is based on only two samples, and it was only possible to determine a value for one of the 70ºC cure

samples. This result does not confirm or dispute either of the proposed theories regarding that to which the event can be attributed. However, there is clearly a small exotherm and hence the most probable effect is post cure shifting the T_g.

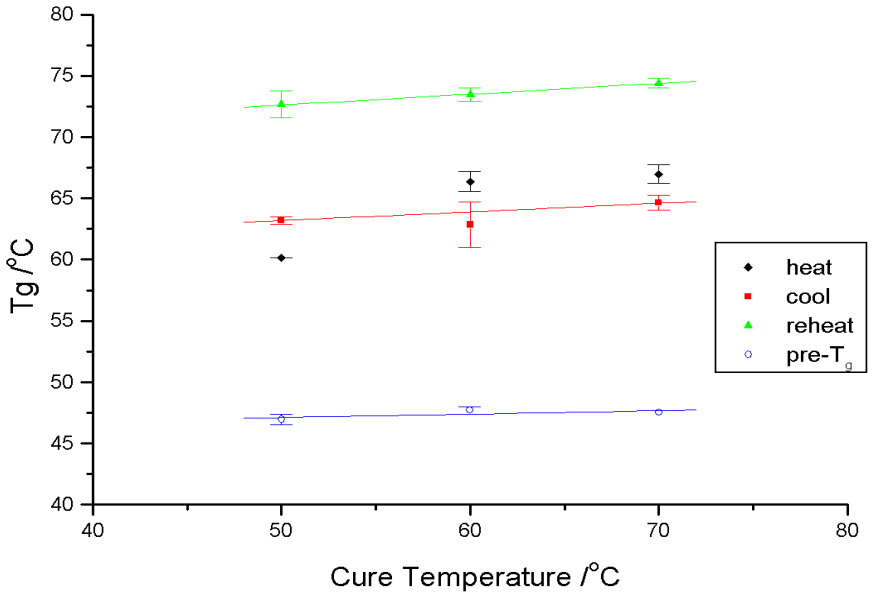

Figure 6. Glass transition temperatures from DSC heat, cool and reheat scans of cured shared model system blocks, as a function of cure temperature.

As for the Prime20 system, the area under the broad exothermic peak seen after the T_g decreases with increasing cure temperature for the heat scan and remains closer to zero for the reheat as expected. This results in a decreasing residual cure. The values from all three repeat scans were used in the calculation of the residual cure, where the value of the dynamic scan used was 488.6 J/g. The results are shown in Table 2.

Table 2. Heat, reheat and residual cure values for the shared model system blocks.

T_c /°C	Scan	Heat (J/g)	Reheat (J/g)	Average Residual Cure
50	repeat1	15.83	0.1536	**2.3%**
	repeat2	10.02	0.4398	
	repeat3	9.246	0.3605	
60	repeat1	9.312	0.447	**1.5%**
	repeat2	9.55	1.222	
	repeat3	6.56	1.087	
70	repeat1	8.251	0.1852	**1.3%**
	repeat2	4.968	0.2566	
	repeat3	6.347	0.4674	

9.3 GRAVIMETRIC ANALYSIS

The three blocks for each sample were immersed in deionised water within sealed beakers. Each beaker was removed individually from the ageing oven, and each block was wiped with tissue immediately prior to being weighed, so that they were weighed within 30 s of being out of the water. Where necessary the water was topped up with fresh deionised water to stop the blocks from drying out. There was no noticeable change in thickness with time, and thickness measurements on a trial sample set of Prime20 aged at 70ºC showed no change in thickness out-with the standard deviation error. Therefore, thickness measurements were not made on the samples used for testing below.

9.3.1 Prime20

9.3.1.1 Aged at 50ºC

Figure 7 shows the plot of the averaged gravimetric results for Prime20 aged at 50ºC, where the cure temperature is represented by a symbol as in the legend. The change in mass has been normalised and plotted on the y-axis, where m_0 is the initial dry mass of the block and $m_t - m_0$ is the mass of water which has ingressed into the block at time t. The error bars represent the standard deviations calculated for each measurement based on the three blocks.

The plot shows that, as expected, as the cure and glass transition temperatures increase the mass of water that has been absorbed by the blocks decreases: 3.3% (T_c=50ºC; T_g=72ºC); 3.2% (T_c=60ºC; T_g=74ºC); 2.7% (T_c=70ºC; T_g=80ºC). The error in the percent uptake in each case which was found by calculating the standard deviation of the three calculated values was approximately 0.01%. The decrease in water uptake for the 70ºC cured material is due to the higher degree of conversion previously illustrated by the increase in T_g with increasing cure temperature. The mass of water absorbed reaches an apparent equilibrium value at long times, reflecting the limited swelling characteristics of crosslinked materials.

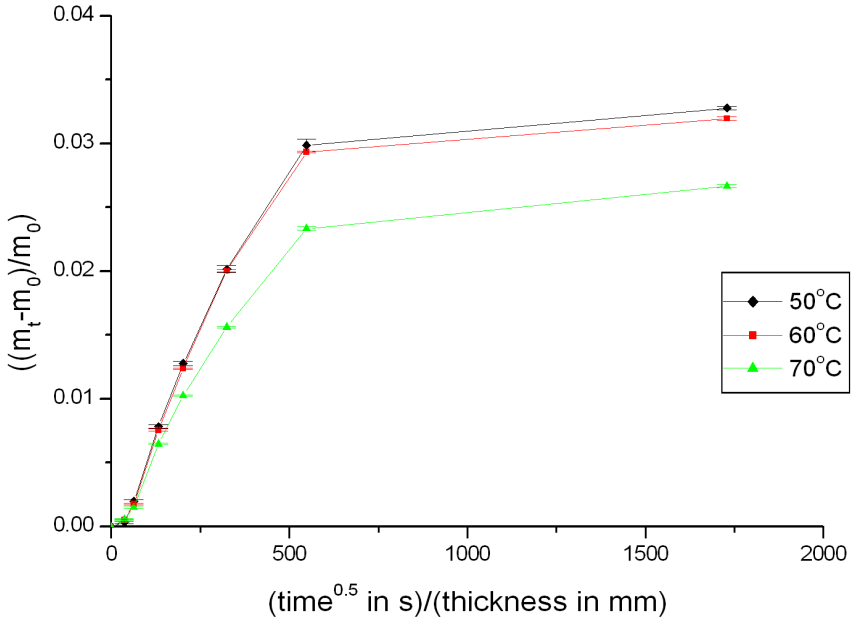

Figure 7. Gravimetric water ingress plot for Prime20 aged at 50ºC, where the legend symbols correspond to the cure temperature (T_c).

Figure 8 shows the gravimetric data presented with the final mass value incorporated into the denominator of the y-axis, where pseudo-Fickian behaviour can be clearly identified. This shows the same shape as seen in Figure 7, except the comparison of the initial slopes is easier to view due to the normalised change in mass.

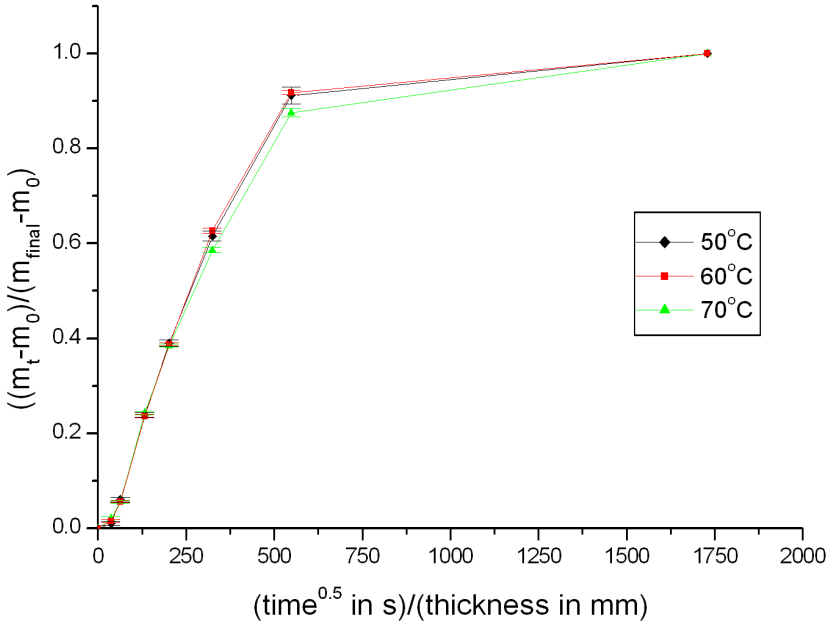

Figure 8. Gravimetric plot incorporating final mass value for Prime20 aged at 50ºC, where the legend symbols correspond to the cure temperature (T_c).

The (gravimetric) diffusion coefficient, D, was calculated using the Boltzmann solution for the initial stage of diffusion (as detailed in *Chapter 2, section 2.5.1, equation 36*) from the initial gradient of the curves shown in Figure 8. The slight initial lag in water uptake is likely to be due to the time taken for any residual mould release still present on the surface of the blocks to be dissolved off in the water before the diffusion of water into the polymer was able to establish in the usual way. The LINEST function within Excel was used to calculate the gradient of the slope between the second time point and the point which lies at *ca*. 0.4 on the y-axis, so as to avoid the lag area. The values for D are shown in Table 3, and show the values of D decreasing slightly as the glass transition temperature (T_g) and cure temperature (T_c) increase, and the percent water decreases. However, when the error is considered the D values are all within the same range. The error was calculated using the error in the slope calculated from the LINEST function and then applying the multiplication of errors method to account for the error in the slope being squared, and so effectively multiplied with itself, within the Boltzmann solution.

Table 3. Gravimetric diffusion coefficient as a function of cure temperature (T_c), glass transition temperature (T_g) and % water uptake for Prime20 blocks aged at 50ºC.

T_c /ºC	T_g /ºC	% uptake	D (x 10^{-7}) /mm^2 s^{-1}
50	71.8 ± 1.5	3.3	10.73 ± 0.48
60	73.9 ± 1.0	3.2	10.50 ± 0.63
70	80.1 ± 1.6	2.7	10.24 ± 0.80

This data set implies that at 50°C (which is ~20°C below the T_g) the diffusion rate is essentially independent of the T_c and the T_g of the material. The amount of water adsorbed does however decrease as the T_g of the material is increased.

9.3.1.2 Aged at 70ºC

Figure 9 shows the plot of the averaged gravimetric results for Prime20 aged at 70ºC, where the cure temperature is represented by a symbol as in the legend. As was shown for the blocks aged at 50ºC, as T_c and T_g increase the percent mass of water ingress decreases: 2.8% (T_c=50ºC; T_g=72ºC); 2.7% (T_c=60ºC; T_g=74ºC); 2.6%

(T_c=70ºC; T_g=80ºC). The percent mass uptake was lower for the samples aged at 70ºC, compared to those aged at 50ºC. The error, based on the standard deviation of the three calculated values, was negligible.

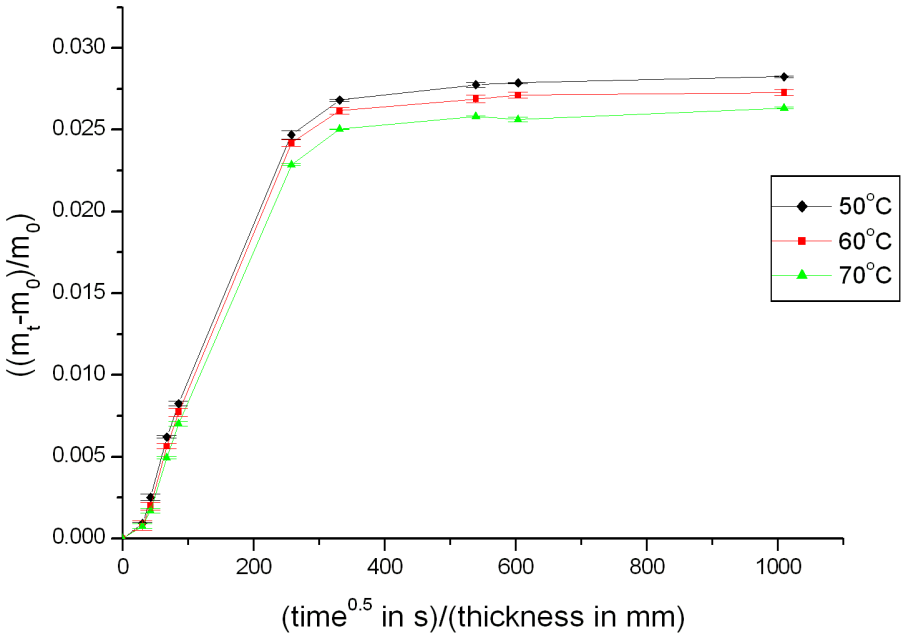

Figure 9. Gravimetric water ingress plot for Prime20 aged at 70ºC, where the legend symbols correspond to the cure temperature (T_c).

Figure 10 shows the gravimetric data presented with the final mass value incorporated into the denominator of the y-axis, where pseudo-Fickian behaviour can be clearly identified.

The (gravimetric) diffusion coefficient, D, was calculated as above using the initial gradient of the curves shown in Figure 10, from the second point to the one which lies just below 0.3 on the y-axis. The values of D are shown in Table 4, and the error was calculated using the method described above. As with the blocks aged at 50ºC, the values of D decrease slightly as the T_g and T_c increase, and the percent water decreases. The observed decrease is more apparent than that for the samples aged at 50°C and the values observed are higher. This reflects the greater ease of diffusion as the T_g is approached. Interestingly, the amount of water absorbed is decreased at the higher temperature, reflecting the effects of thermodynamics on the water solubility in the matrix.

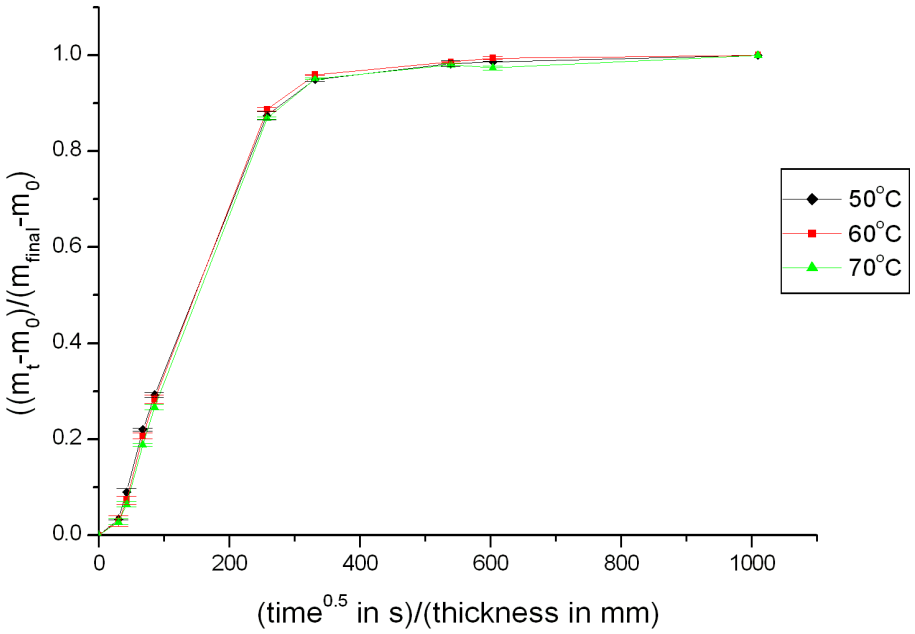

Figure 10. Gravimetric plot incorporating final mass value for Prime20 aged at 70ºC, where the legend symbol corresponds to the cure temperature (T_c).

Table 4. Gravimetric diffusion coefficient as a function of cure temperature (T_c), glass transition temperature (T_g) and % water uptake for Prime20 blocks aged at 70ºC.

T_c /ºC	T_g /ºC	% uptake	D (x 10^{-7}) /mm^2 s^{-1}
50	71.8 ± 1.5	2.8	45.02 ± 2.28
60	73.9 ± 1.0	2.7	44.26 ± 2.89
70	80.1 ± 1.6	2.6	38.93 ± 2.87

9.3.2 Shared Model System

9.3.2.1 Aged at 50ºC

Figure 11 shows the plot of the averaged gravimetric results for the shared model system aged at 50ºC, where the cure temperature is represented by a symbol as in the legend. The error bars represent the standard deviations calculated for each measurement based on the three blocks. The error bar for the samples cured at 50ºC are significantly higher than for the other cure temperatures, particularly near equilibrium. This is believed to be due to one of the blocks (of the three) being slightly different from the other two – either in homogeneity of epoxy-amine mixture throughout block or void level. However, this was not investigated further. The plot

shows that as the cure temperature increases the mass of water that has been absorbed by the blocks decreases slightly: 2.4% (T_c=50ºC; T_g=60ºC); 2.3% (T_c=60ºC; T_g=66ºC); 2.3% (T_c=70ºC; T_g=67ºC). The error in the percent uptake in each case which was found by calculating the standard deviation of the three calculated values was less than 0.01% for the samples cured at 60ºC and 70ºC, and was 0.2% for those cured at 50ºC. With consideration to the error there would not appear to be significant difference between the three percent water uptake values.

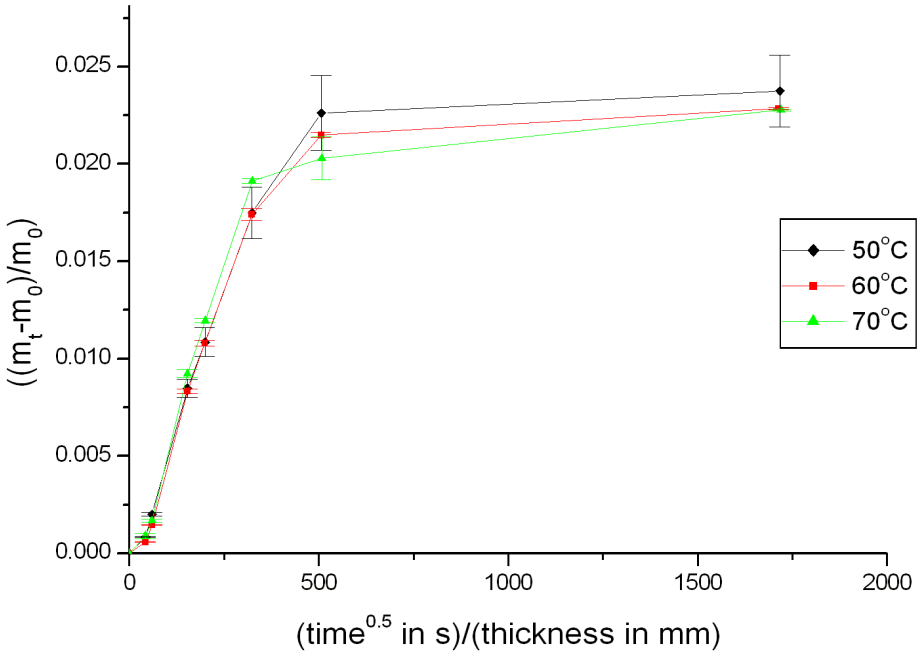

Figure 11. Gravimetric water ingress plot for shared model system aged at 50ºC, where the legend symbols correspond to the cure temperature (T_c).

Figure 12 shows the gravimetric data presented with the final mass value incorporated into the denominator of the y-axis, where pseudo-Fickian behaviour can be clearly identified. The (gravimetric) diffusion coefficient, D, was calculated as above using the initial gradient of the curves shown in Figure 12, from the second point to the one which lies at *ca.* 0.5 on the y-axis. The values of D are shown in Table 5, and the error was calculated using the method described above. Contrary to what was observed with the Prime20 blocks, the values of D increase as the T_g and T_c increase, and the percent water decreases slightly. This increase in D cannot be accounted for within the calculated error in this case. The values of D are higher

than those for the Prime20 system also aged at 50°C – this can in part be attributed to the significantly lower values of the T_g. However, this system has the potential of producing a more highly crosslinked matrix than Prime20 and as such the possibility of densification is limited by the crosslinking process. Changes in the nature of the structure of material are also reflected in lower values of the % water uptake compared with those for the Prime20 material.

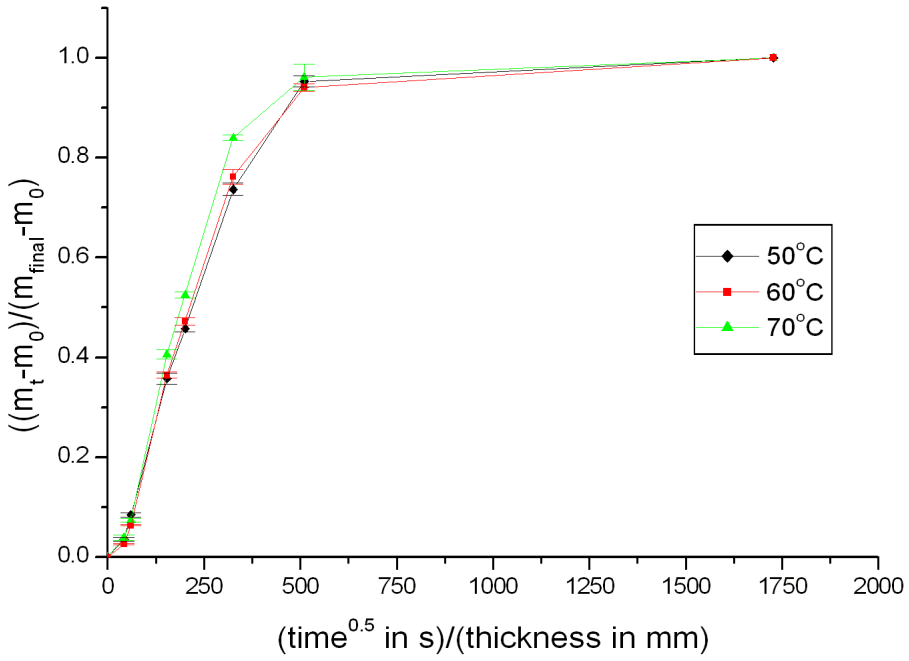

Figure 12. Gravimetric plot incorporating final mass value for shared model system aged at 50ºC where the legend symbols correspond to the cure temperature (T_c).

Table 5. Gravimetric diffusion coefficient as a function of cure temperature (T_c), glass transition temperature (T_g) and % water uptake for shared model system blocks aged at 50ºC.

T_c /ºC	T_g /ºC	% uptake	D (x 10^{-7}) /mm^2 s^{-1}
50	60.1 ± 0.0*	2.4	14.46 ± 0.78
60	66.4 ± 0.8	2.3	16.68 ± 1.01
70	67.0 ± 0.8	2.3	19.92 ± 1.27

*calculated error less than 0.01ºC.

9.3.2.2 Aged at 70ºC

Figure 13 shows the plot of the averaged gravimetric results for the shared model system aged at 70ºC. The plot shows that as the cure temperature increases from 50ºC to 60ºC the mass of water that has been absorbed by the blocks decreases

slightly, and then remains the same at 70ºC: 2.7% (T_c=50ºC; T_g=60ºC); 2.2% (T_c=60ºC; T_g=66ºC); 2.2% (T_c=70ºC; T_g=67ºC). The error in each case was less than 0.02%, and so the decrease in precentage uptake between the blocks with a T_g of 60ºC, and those with a higher T_g cannot be attributed to error.

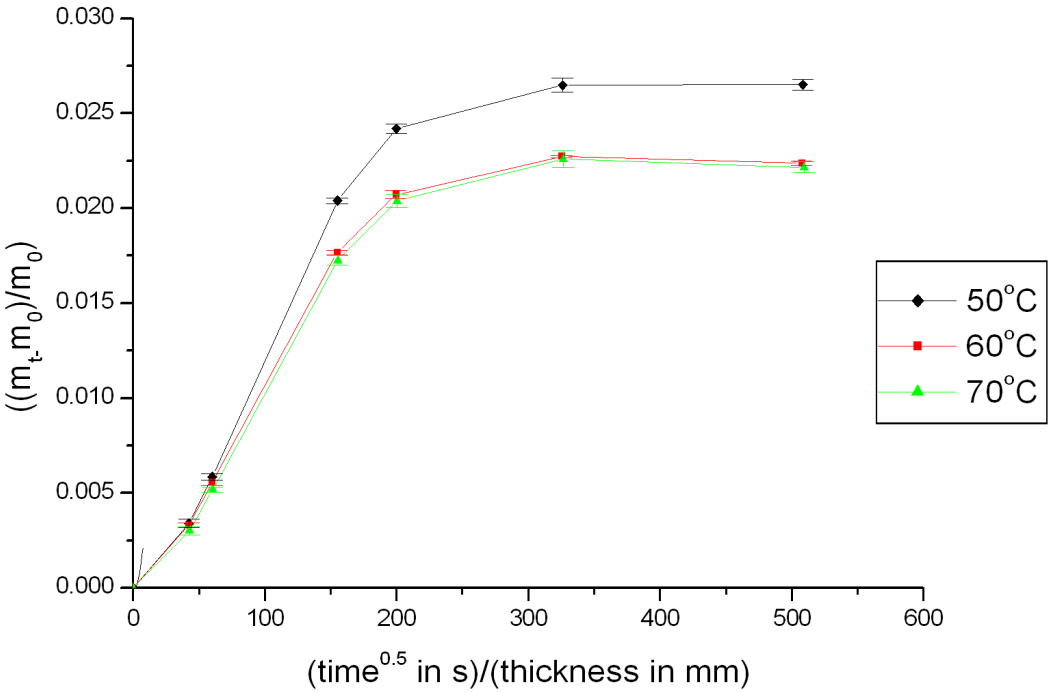

Figure 13. Gravimetric water ingress plot for shared model system aged at 70ºC, where the legend symbols correspond to the cure temperature (T_c).

The (gravimetric) diffusion coefficient, D, was calculated as above using the initial gradient of the curves shown in Figure 14, from the second point to the one which lies at *ca.* 0.8 on the y-axis.

The values of D are shown in Table 6, and the error was calculated using the method described above. The high values of D reflect the high mobility of the water molecules in a matrix which is above its T_g. The lower level of moisture uptake reflects the influence of thermodynamic factors on the diffusion processes.

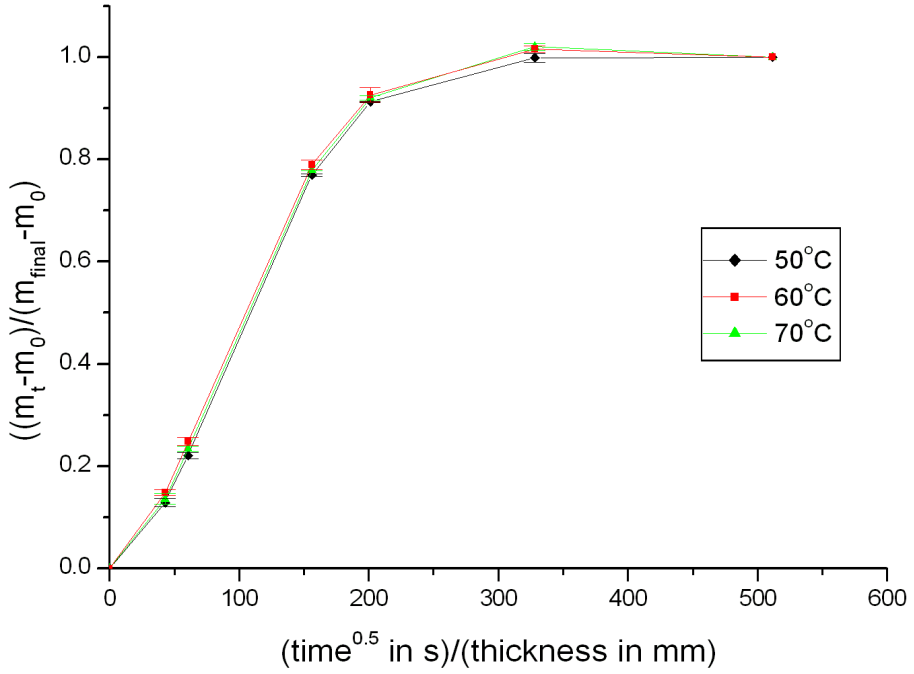

Figure 14. Gravimetric plot incorporating final mass value for shared model system aged at 70ºC, where the legend symbols correspond to the cure temperature (T_c).

Table 6. Gravimetric diffusion coefficient as a function of cure temperature (T_c), glass transition temperature (T_g) and % water uptake for shared model system blocks aged at 70ºC.

T_c /ºC	T_g /ºC	% uptake	D (x 10^{-7}) /mm^2 s^{-1}
50	60.1 ± 0.02	2.7	63.50 ± 1.17
60	66.4 ± 0.8	2.2	63.01 ± 0.07
70	67.0 ± 0.8	2.2	63.58 ± 0.39

9.3.3 Gravimetric Conclusions

Blocks of Prime20 and the shared model system were cured at 50ºC, 60ºC and 70ºC, and then aged in water held at either 50ºC or 70ºC. Figure 15 below compares the percent water uptake against the cure temperature for each sample. Error bars are based on the standard deviations, and where no error bars are shown the errors were less than 0.01%. The plot shows that in general the percent of water ingress decreased with increasing cure temperature, and that the Prime20 samples absorbed more water than the shared model system samples. The differences in the observed behaviour can be attributed to changes in the T_g and the matrix, and also to the thermodynamics of the interaction of the matrix with water. The latter effect can be

directly related to the chemical structure of the resin used - this will be discussed in more detail at the end of this chapter.

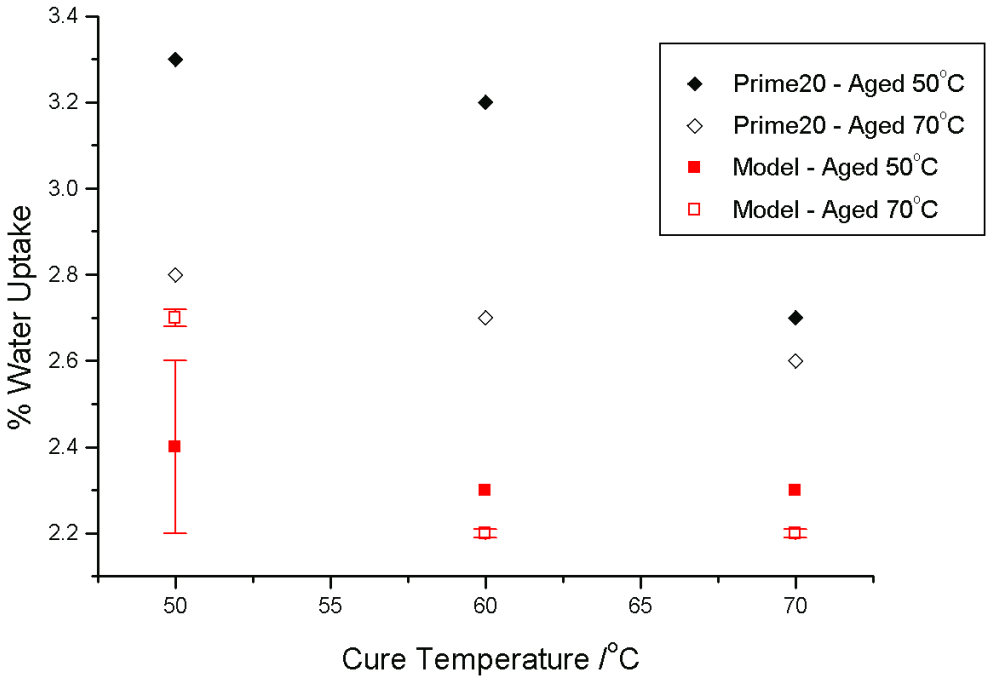

Figure 15. Comparison of percent water uptake for Prime20 and shared model system at different cure and ageing temperatures.

When the percent water uptake is plotted against the T_g, as in Figure 16 (where error bars are not visible, the calculated error was negligible), it is more clearly seen that the water uptake decreases with increasing T_g (which was influenced by the T_c). It is also more clearly shown that for the shared model system there is very little difference in the T_g between the blocks cured at 60ºC and 70ºC, and as a result there is very little difference in the water uptake.

Figure 17 compares the calculated diffusion coefficient, D, against the T_c. For both systems the samples aged at the higher temperature had a higher D value. The D value decreased with increasing cure temperature, as expected, for the Prime20 samples. However, with the shared model system, the samples aged at 50ºC showed an increase in D with increasing T_c, but remained almost constant when aged at 70ºC. This can be more clearly seen in Figure 18, where the D value is plotted against T_g.

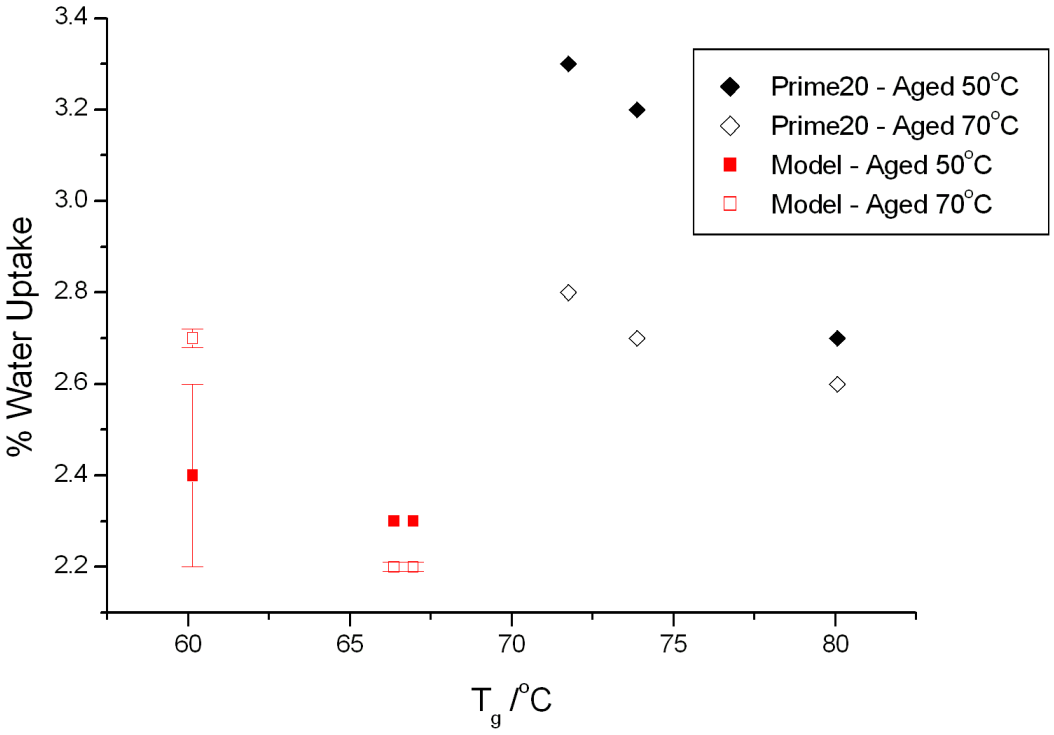

Figure 16. Comparison of percent water uptake for Prime20 and shared model system at different ageing temperatures against the glass transition temperature (T_g).

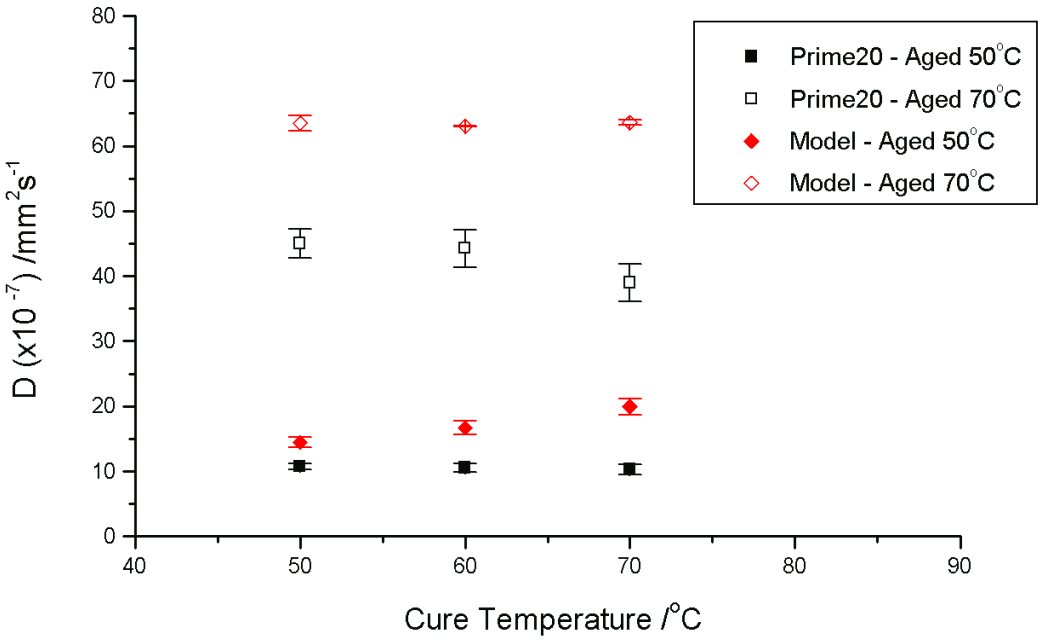

Figure 17. Comparison of D values for Prime20 and shared model system at different cure and ageing temperatures.

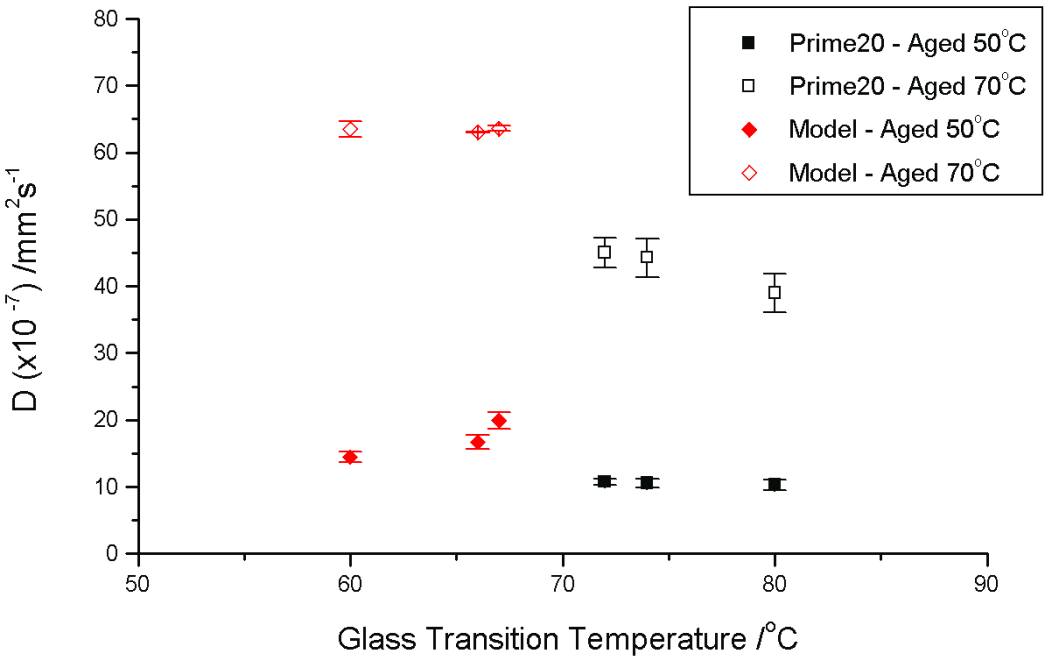

Figure 18. Comparison of D values for Prime20 and shared model system at different ageing temperatures against the glass transition temperature (T_g).

9.4 HIGH FREQUENCY DIELECTRICS

The high frequency dielectric spectrometer, which was used to assess the free water, scanned from ca. 10MHz to 10GHz with the sample held against the probe. There were three blocks of each type of sample (e.g. Prime20 cured at 50ºC and aged at 70ºC would be a sample) and five measurements were made on each of those blocks giving a total of fifteen measurements on each type of sample. The average of these was used in the plots below, and the standard deviations used for the error.

9.4.1 Prime20

9.4.1.1 Aged at 50ºC

Figure 19 shows the high frequency response for the Prime20 samples cured and aged at 50ºC - similar plots for samples cured at 60ºC and 70ºC (and also aged 50ºC) at can be found in the Appendices. It is difficult to extract useful information to follow what is happening as the time increases from these raw data plots. The

oscillatory behaviour at low frequency (50 MHz – 200 MHz) is partly a consequence of the measurements being achieved using an end of line approach.

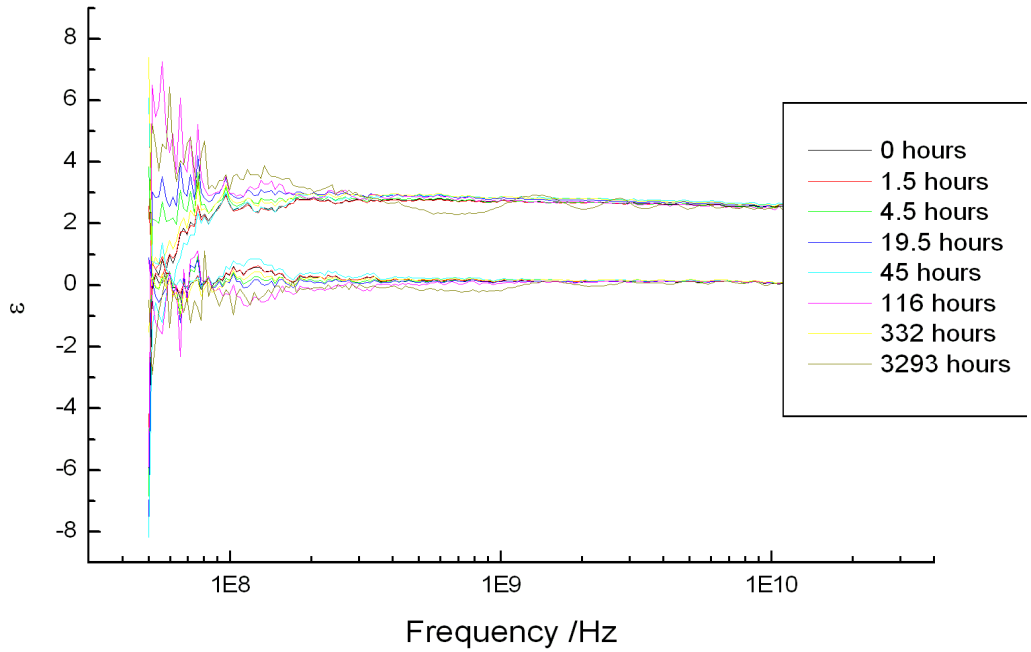

Figure 19. Changes in real permittivity (top set of lines) and imaginary permittivity (bottom) against frequency for Prime20 cured and aged at 50°C (legend indicates exposure time).

The method involves an analysis of the impendence change as a function of frequency and is susceptible to the effects of change in the load on the end of the line and changes in the wave pattern which is created in the waveguide. The values of the (real) permittivity obtained at a frequency of 1.28 x 10^{10} Hz are a true reflection of the changes in the permittivity of the media, not being influenced by the standing waves in the waveguide, and have therefore been chosen to follow the dipolar relaxation associated with 'free' water.

Figure 20 shows the change in real permittivity as a result of 'free' water. The permittivity initially does not increase significantly, with the values staying constant over the first 4.5 hours of exposure. During the next period to 45 hours the value of the permittivity increases. This change would be consistent with water having diffused to regions which contain voids of sufficient size for the water molecules to cluster and exhibit the fast relaxation associated with bulk water. The apparent

increase in the permittivity is a reflection of the existence of such a void structure within the resin.

The observed drop in the value of the permittivity after 116 hours and the subsequent fall below the initial value is a consequence of the collapse of the voids when the matrix has become plasticized by the ingress of moisture. It should be noted that this drop is greater at the higher temperature of cure where we would expect there to be a more open matrix created initially. The moisture is not lost but is moving into the matrix and becoming molecularly dispersed water. This effect has been observed previously with other epoxy systems.

The rise from 332 hours exposure followed by a decrease again (both above initial starting value) reflects the filling of the voids as a dynamic process or that voids are being created and destroyed during that water uptake process.

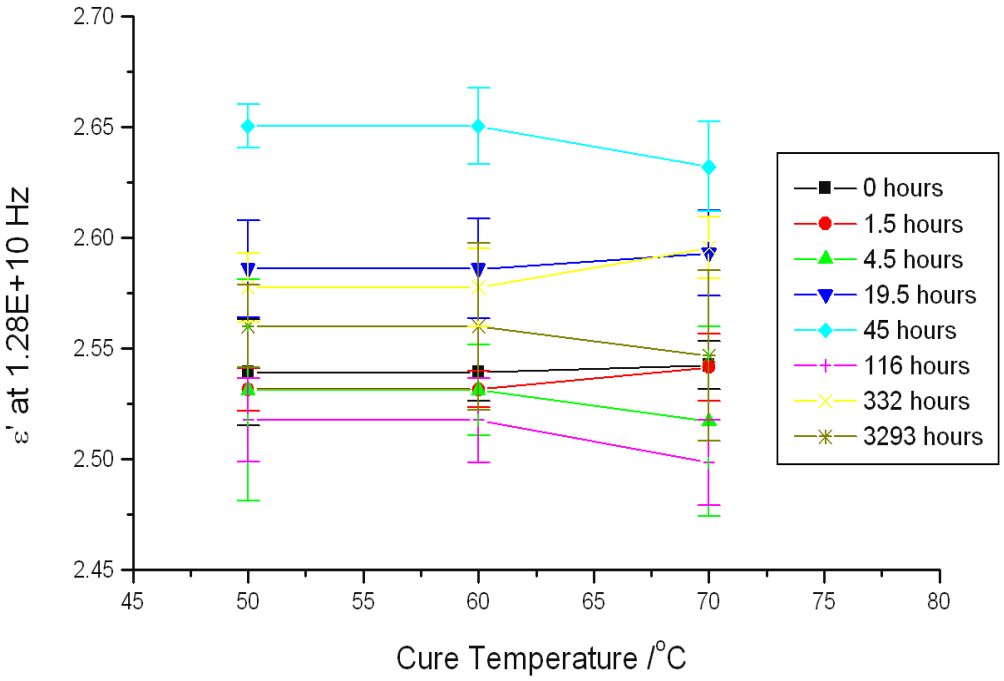

Figure 20. Plot showing change in real permittivity as a result of 'free' water for Prime20 samples aged at 50°C.

9.4.1.2 Aged at 70ºC

The plots showing the high frequency response over the full range of frequencies for samples cured at 50ºC, 60ºC and 70ºC, and then aged at 70ºC can be found in the Appendices. Figure 21 shows the (real) permittivity changes associated with free water. The high frequency data for the 70°C aged samples follows similar trends as observed at 50°C except that there is initially a slight increase, and the largest contribution is observed after 401 hours (compared to 45 hours for 50°C aged samples). After this point it again falls to a lower value, but does not fall below the initial value for the permittivity. The variation reflects the filling of void structures and their collapse, however the rate at which this occurs and the extent to which water in the voids redistributes is different from that observed at the lower aging temperature.

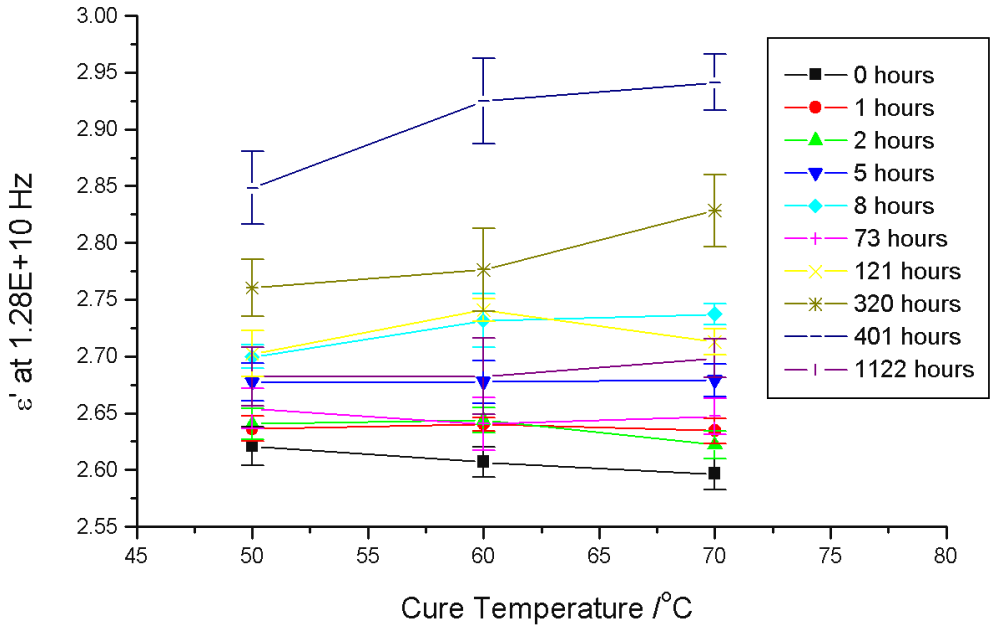

Figure 21. Plot showing change in real permittivity as a result of 'free' water for Prime20 samples aged at 70°C.

9.4.2 Shared Model System

9.4.2.1 Aged at 50ºC

Plots showing the response over the full range of frequencies for samples cured at 50ºC, 60ºC and 70ºC, and then aged at 50ºC can be found in the Appendices. The

model system is more highly crosslinked than Prime20 and the ability for molecular sized voids to form is therefore less than with the previous resin system. The changes in the high frequency permittivity are therefore correspondingly smaller. The variations are not as clear but the same general effects are observed; an initial increase followed by a reduction, followed by subsequent rises and falls reflecting the filling of the voids is a dynamic process or that voids are being created and destroyed during that water uptake process.

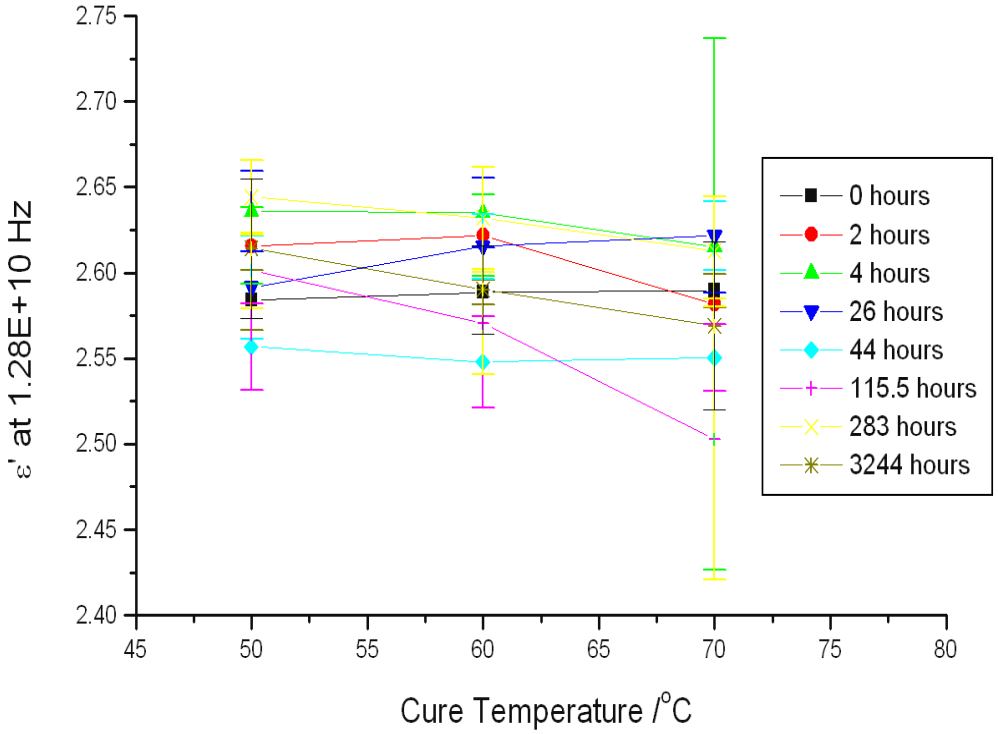

Figure 22. Plot showing change in real permittivity as a result of 'free' water for the shared model system samples aged at 50°C.

9.4.2.2 Aged at 70ºC

Plots showing the response over the full range of frequencies for samples cured at 50ºC, 60ºC and 70ºC, and then aged at 70ºC can be found in the Appendices. As at 50°C, the variation is lower than for Prime20, and there is no clear trend - once more reflecting the complex way in which voids are being filled and emptied with time as a consequence of changes in the dynamics of the matrix which form the walls of the voids.

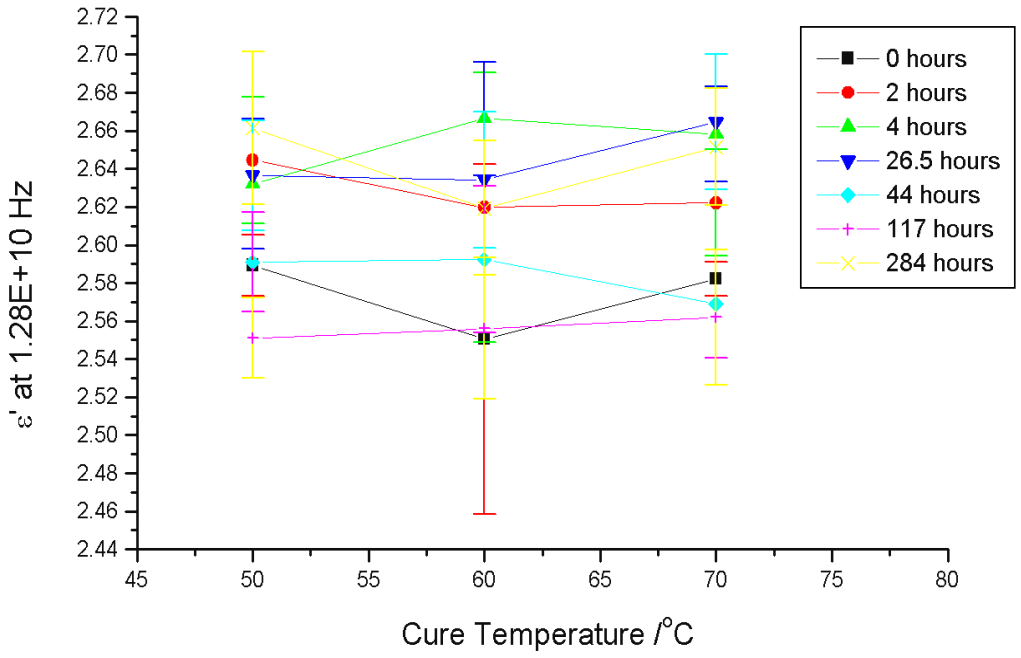

Figure 23. Plot showing change in real permittivity as a result of 'free' water for the shared model system samples aged at 70°C.

9.4.3 High Frequency Dielectrics Conclusions

Both systems show the same general trends with an initial increase in permittivity followed by a decrease, reflecting the filling of voids with 'free' water and the subsequent collapse of the void structure. Smaller changes were observed in the shared model system as a result of it being less crosslinked and therefore having less ability for molecular sized voids to form than the Prime20 system.

9.5 MID FREQUENCY DIELECTRICS

The Novotronic spectrometer used scanned from 1Hz to 1MHz on each of the three blocks (per sample). The average of the three results was used in the plots below, and the standard deviations used in the calculation of the errors. In the mid frequency range the water molecules are bound to the resin matrix and can be associated with the pendant hydroxyl groups created during the cure reaction. Bound water will result in a shift in the permittivity within the frequency range scanned.

9.5.1 Prime20

9.5.1.1 Aged at 50ºC

Figure 24 shows the permittivity changes across the frequency range scanned at each time interval for Prime20 cured and aged at 50ºC – the top set of data is the real permittivity (ε') and the bottom set is the imaginary permittivity (ε"). The step that can be seen at 2Hz was evident on all of the samples run and is believed to be due to a slight shift in calibration files. The plots for the samples cured at 60ºC and 70ºC can be found in the Appendices.

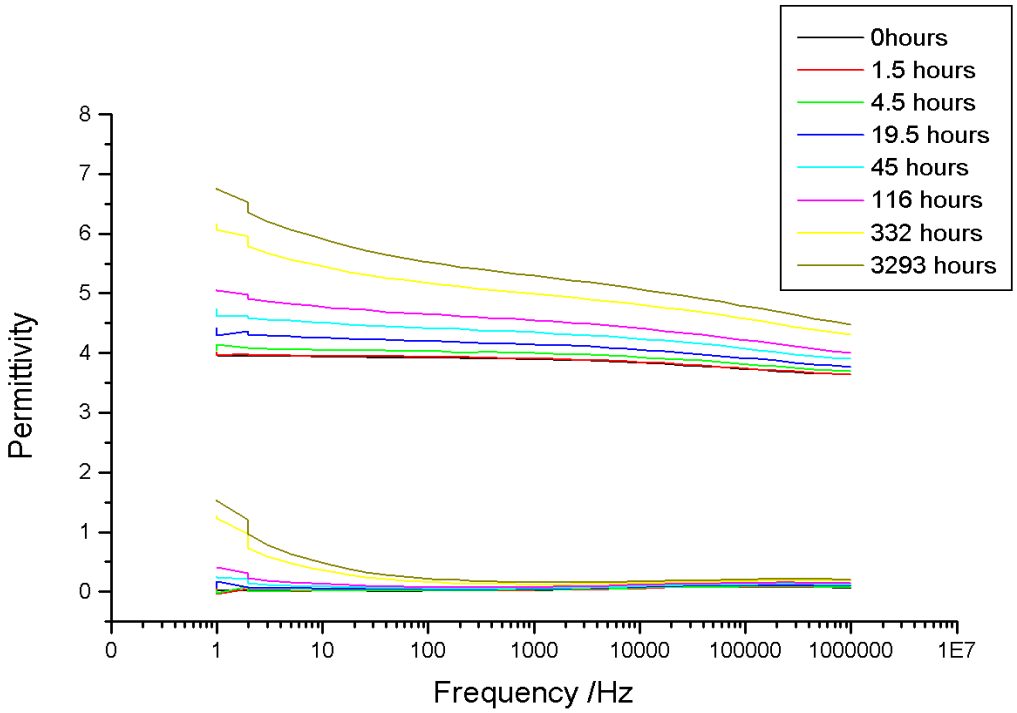

Figure 24. Changes in real permittivity (top set of lines) and imaginary permittivity (bottom) against frequency for Prime20 cured and aged at 50ºC (legend indicates exposure time).

An increase in permittivity at approximately 1 kHz would be expected as a result of water uptake in the blocks. Figure 25 and Figure 26 show the changes in real and imaginary permittivity respectively at 1 kHz, where the error was calculated using the addition of errors method. The plots do not plateau as demonstrated in the gravimetric plots - this could be a result of swelling. There was no noticeable change in thickness, and thickness measurements on a trial sample set of Prime20 aged at 70ºC showed no change in thickness out-with the standard deviation error. Therefore, the calibration settings in the instrument were not adjusted from the initial

settings for each sample. The shape of the permittivity against time plots resemble those for the gravimetric water plots.

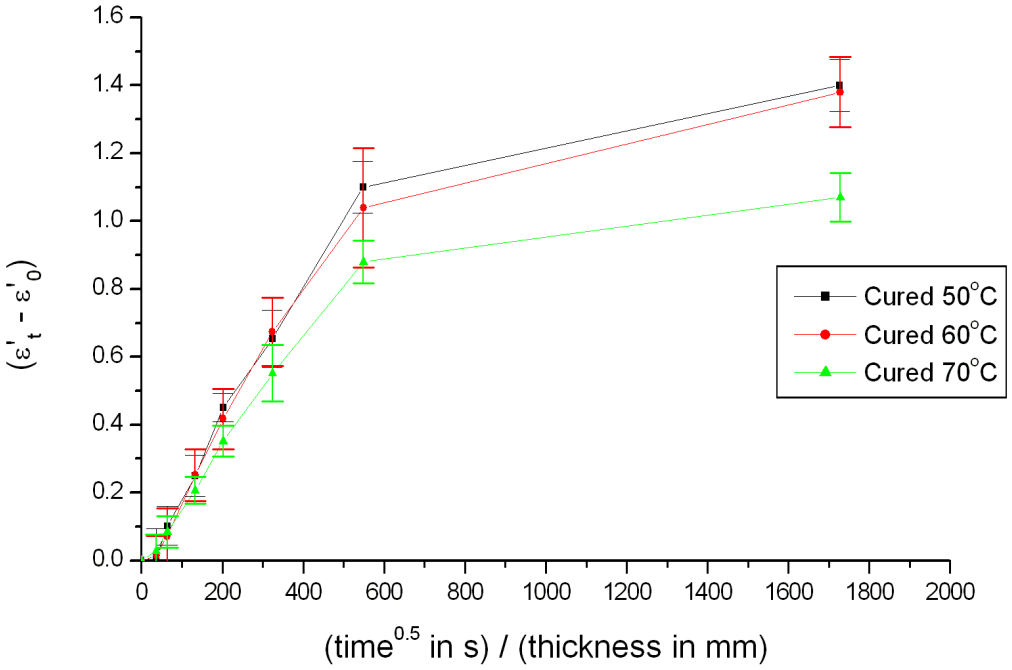

Figure 25. Changes in real permittivity at 1 kHz as a result of water ingress for Prime20 aged at 50ºC.

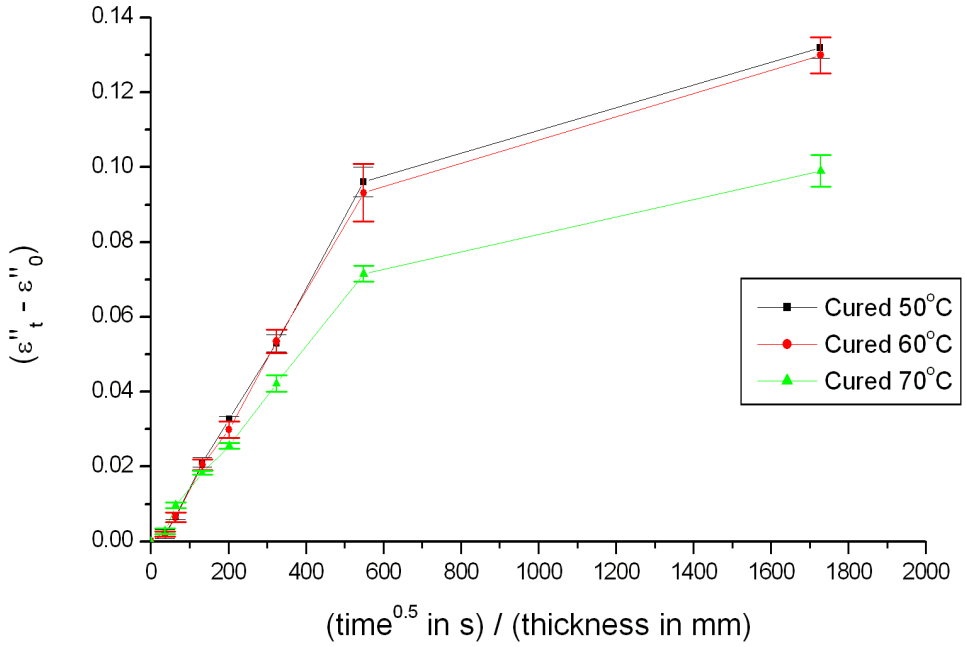

Figure 26. Changes in imaginary permittivity at 1 kHz as a result of water ingress for Prime20 aged at 50ºC.

9.5.1.2 Aged at 70ºC

Figure 27 shows the permittivity changes across the frequency range scanned as a result of water uptake for Prime20 cured at 50ºC and aged at 70ºC. The plots for the blocks cured at 60ºC and 70ºC can be found in the Appendices. Figure 28 and Figure 29 show the changes in real and imaginary permittivity respectively at 1 kHz as a result of water ingress. As with the blocks aged at 50ºC, the plots do not plateau as demonstrated in the gravimetric plots – this is attributed to swelling.

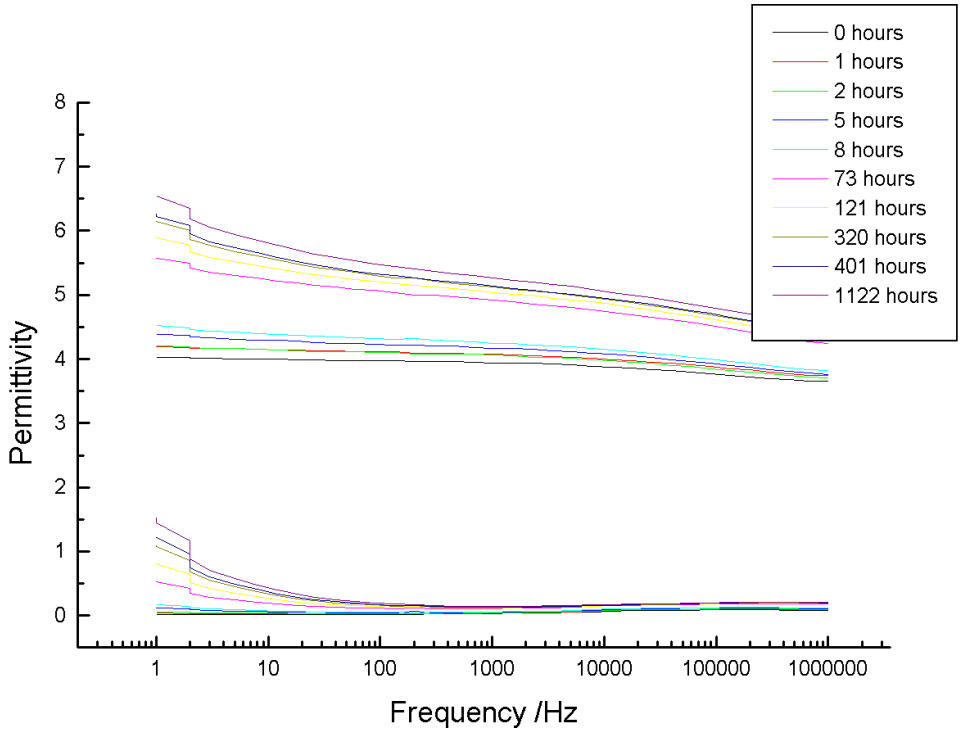

Figure 27. Changes in real permittivity (top set of lines) and imaginary permittivity (bottom) against frequency for Prime20 cured at 50ºC and aged at 70ºC (legend indicates exposure time).

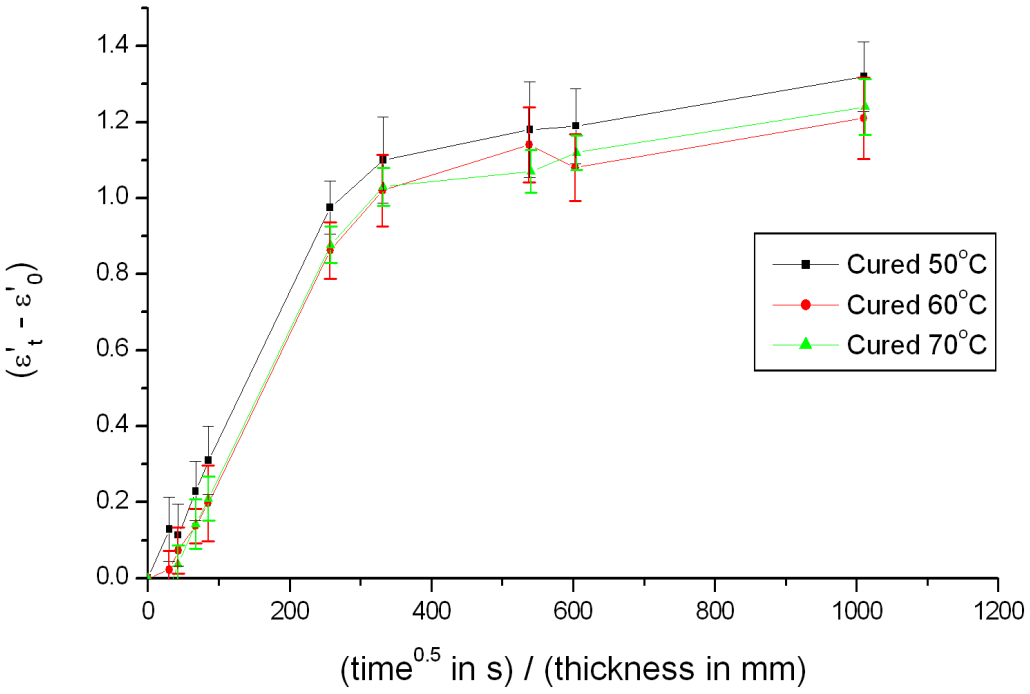

Figure 28. Changes in real permittivity at 1 kHz as a result of water ingress for Prime20 aged at 70ºC.

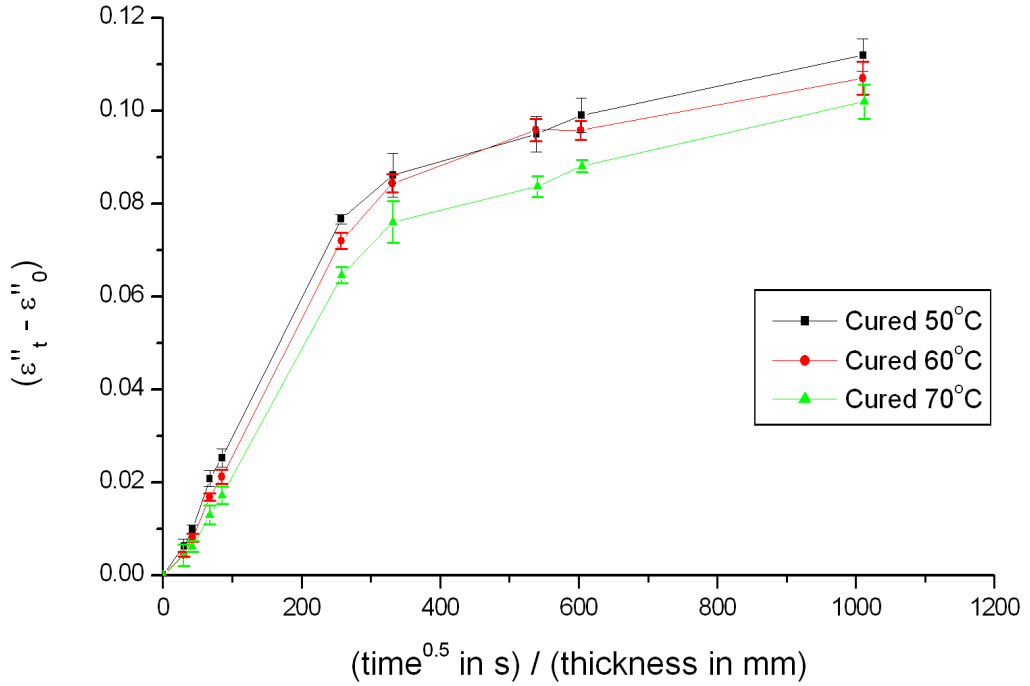

Figure 29. Changes in imaginary permittivity at 1 kHz as a result of water ingress for Prime20 aged at 70ºC.

9.5.2 Shared Model System

9.5.2.1 Aged at 50ºC

Figure 30 shows the permittivity changes across the frequency range scanned as a result of water uptake for the shared model system cured at 50ºC and aged at 50ºC. The plots for the blocks cured at 60ºC and 70ºC can be found in the Appendices.

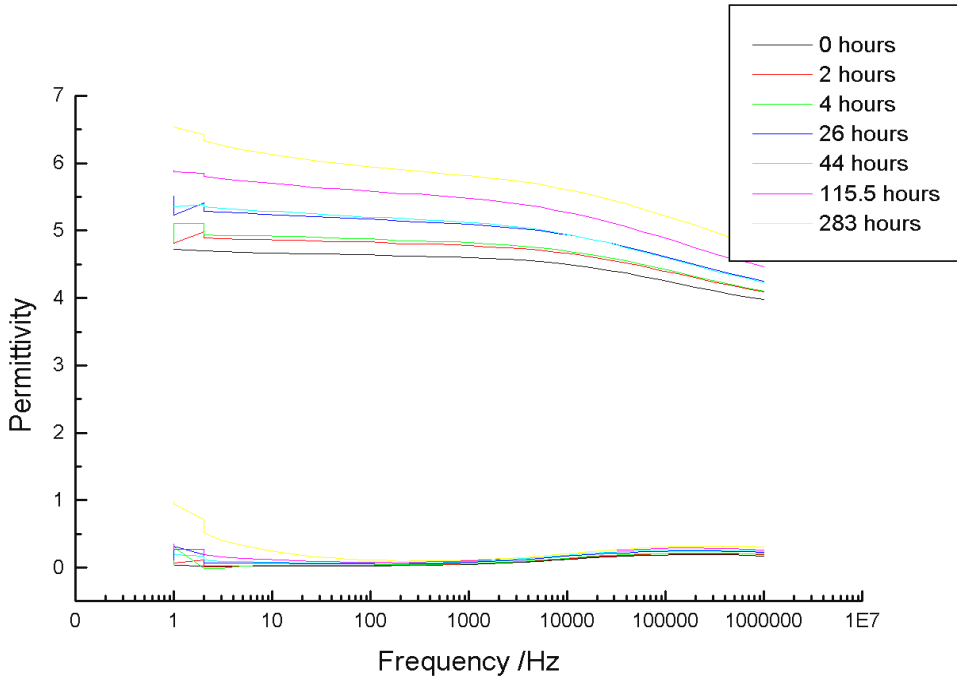

Figure 30. Changes in real permittivity (top set of lines) and imaginary permittivity (bottom) against frequency for the shared model system cured and aged at 50ºC (legend indicates exposure time).

Figure 31 and Figure 32 show the changes in real and imaginary permittivity respectively at 1 kHz as a result of water ingress. For the last measurement at 3244.5 hours there was a problem with the instrument - no results were generated for 50ºC. The results from 60ºC and 70ºC appear to show a decrease in water uptake over the final data points – more apparent in the real permittivity data – this could be a result of plasticisation of the epoxy resin, allowing densification and hence the moisture loss in the sample. Plasticization of the matrix would allow the chains to adopt a more favorable conformation and the matrix would adopt a denser structure. The closer packing of the chains would exclude the water molecules and hence there would be a lower value of the permittivity observed.

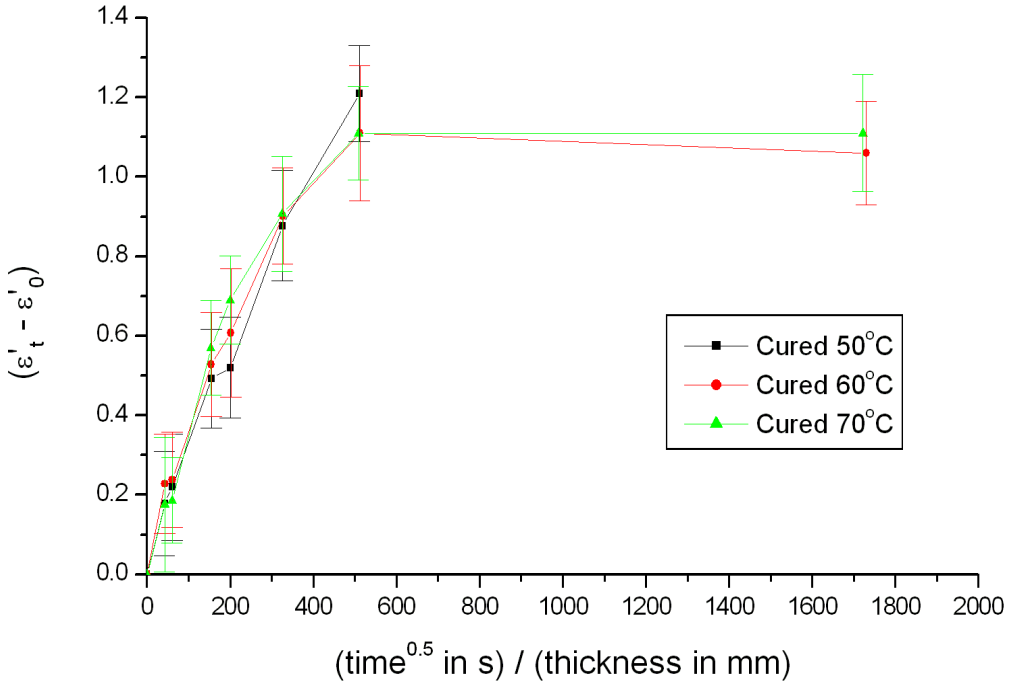

Figure 31. Changes in real permittivity at 1 kHz as a result of water ingress for the shared model system aged at 50ºC.

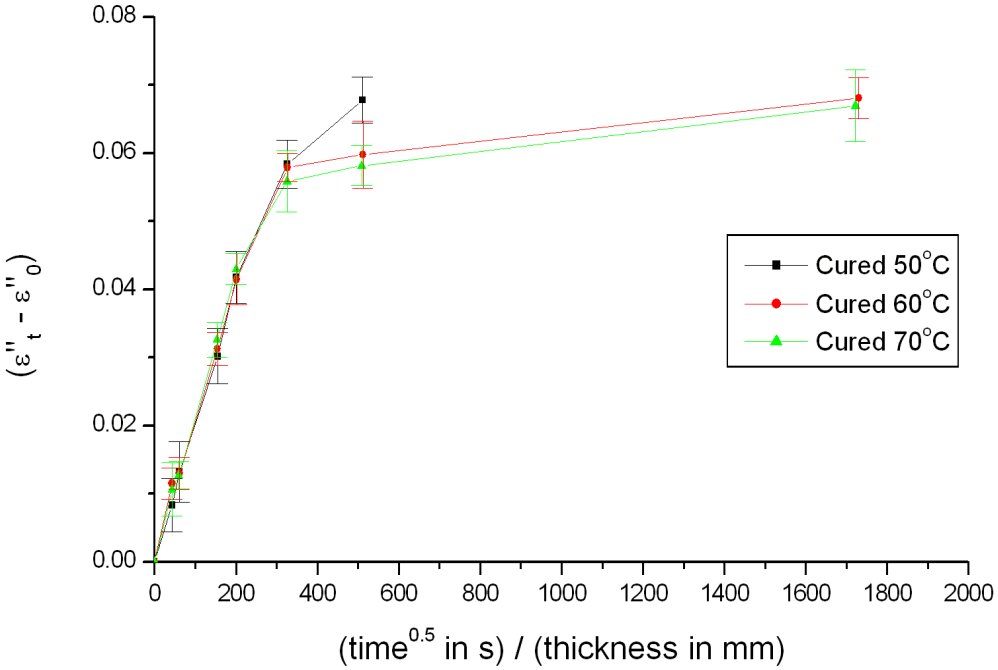

Figure 32. Changes in imaginary permittivity at 1 kHz as a result of water ingress for the shared model system aged at 50ºC.

9.5.2.2 Aged at 70ºC

Figure 33 shows the permittivity changes across the frequency range scanned as a result of water uptake for the shared model system cured at 50ºC and aged at 70ºC. The plots for the blocks cured at 60ºC and 70ºC can be found in the Appendices.

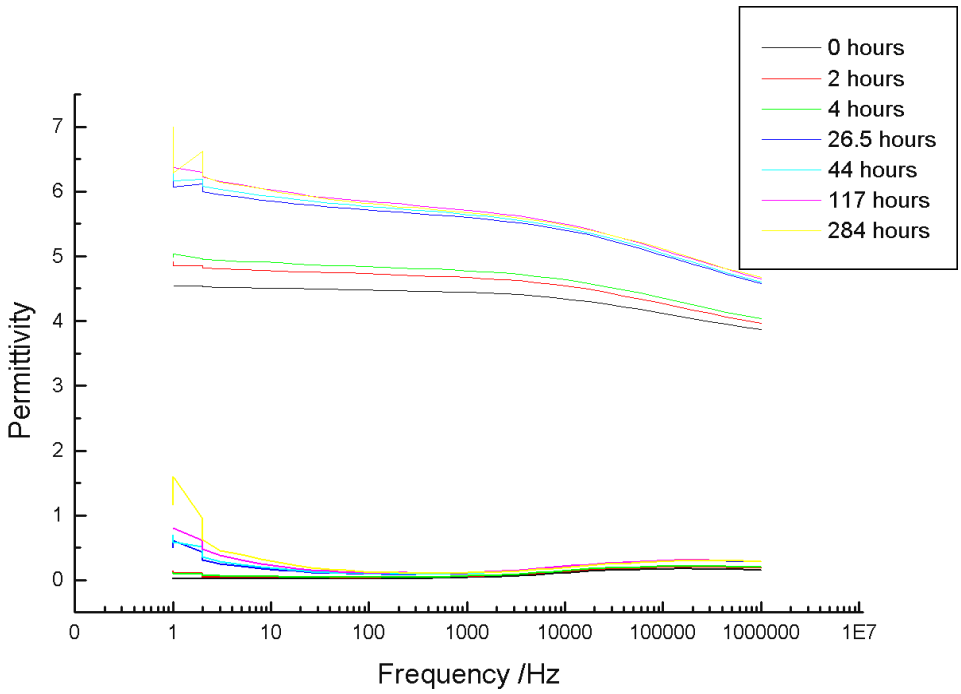

Figure 33. Changes in real permittivity (top set of lines) and imaginary permittivity (bottom) against frequency for shared model system cured at 50ºC and aged at 70ºC (legend indicates exposure time).

Figure 34 and Figure 35 show the changes in real and imaginary permittivity respectively at 1 kHz as a result of water ingress. The results from 50ºC cure shows a slight decrease values over the final points, whereas 60ºC and 70ºC cure appear to show a continued increase in water uptake over the final data.

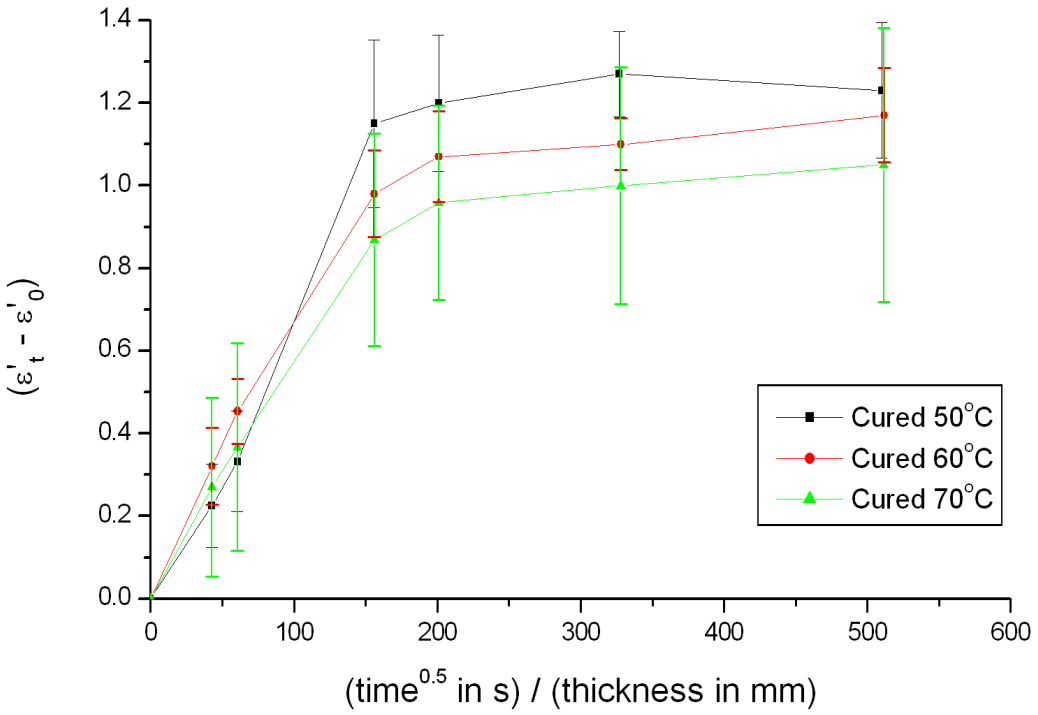

Figure 34. Changes in real permittivity at 1 kHz as a result of water ingress for the shared model system aged at 70ºC.

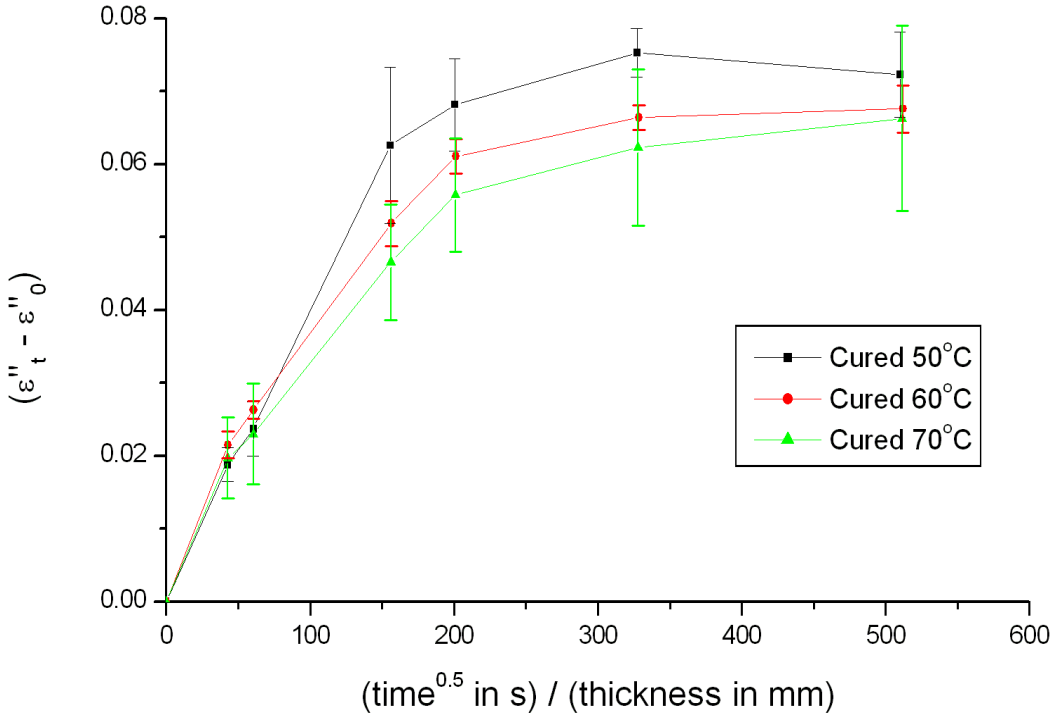

Figure 35. Changes in imaginary permittivity at 1 kHz as a result of water ingress for the shared model system aged at 70ºC.

9.6 COMPARISON OF ANALYSIS METHODS

The gravimetric data and dielectric measurements show a progressive increase with time reflecting the moisture entering the matrix. An estimated percent uptake of water can be calculated from the dielectrics data by dividing the increment from the equilibrium ε' values by 80 (permittivity of water), and converting to a percentage. These values are displayed in Table 7 for Prime20 aged at 50°C. The dielectric results would indicate that the amount of water which is absorbed is ~ 1.6%, compared to a value of ~ 3.1% from the gravimetric data; with the trend being a decrease in water uptake with increasing cure temperature (for both measurement methods).

Table 7. Water ingress data for Prime20 aged at 50°C.

T_c /°C	Gravimetric % uptake	Equilibrium $\varepsilon'_t - \varepsilon'_0$ values	Estimated % uptake from $\varepsilon'_t - \varepsilon'_0$ value	Kirkwood coefficient
50	3.3	1.40	1.75	0.53
60	3.2	1.38	1.73	0.54
70	2.7	1.07	1.34	0.50

The estimates were made on the basis that 80 is the permittivity for water. This value of 80 is for a freely rotating dipole and restriction of the freedom of the water molecule by being bound to the pendant hydroxyl group would be expected to influence the observed increment [4]. The scaling factor which is usually used to directly compare the estimated value with the value obtained from the gravimetric measurements is the Kirkwood coefficient. This value can be found for each cure temperature in Table 7, with the average scaling factor is ~ 0.52.

The values for Prime20 aged at 70°C are displayed in
Table **8**. The dielectric results indicate ~ 1.6% water uptake, compared to a value of ~ 2.7% from the gravimetric data, and a scaling factor of ~ 0.58. The gravimetric results show a decrease in water ingress at the higher aging temperature of 70°C compared to those aged at 50°C. This could be as a result of the higher aging temperature being closer to the observed T_g. The estimated percent uptake from the

dielectrics data shows a smaller change for blocks aged at 70°C compared to those aged at 50°C.

Table 8. Water ingress data for Prime20 aged at 70°C.

T_c /ºC	Gravimetric % uptake	Equilibrium $\varepsilon'_t - \varepsilon'_0$ values	Estimated % uptake from $\varepsilon'_t - \varepsilon'_0$ value	Kirkwood coefficient
50	2.8	1.32	1.66	0.59
60	2.7	1.21	1.51	0.56
70	2.6	1.24	1.55	0.60

The values for the shared model system aged at 50°C are displayed in Table 9. As previously discussed the final value for the blocks cured at 50°C was not taken. It is likely that this would have shown a decrease in permittivity as seen for the blocks cured at 60°C and 70°C, which would have resulted in a lower estimated percent uptake and scaling factor. Discounting the values shown for the 50°C cured blocks, the dielectric results indicate ~ 1.4% water uptake, compared to a value of ~ 2.3% from the gravimetric data, and a scaling factor of ~ 0.59 for the shared resin blocks aged at 50°C.

Table 9. Water ingress data for the shared system at 50°C.

T_c /ºC	Gravimetric % uptake	Equilibrium $\varepsilon'_t - \varepsilon'_0$ values	Estimated % uptake from $\varepsilon'_t - \varepsilon'_0$ value	Kirkwood coefficient
50	2.4	1.21*	1.51	0.63
60	2.3	1.06	1.33	0.58
70	2.3	1.11	1.39	0.60

*This value is for the measurement at 283 hours, as no measurement was made at 3244.5 hours.

The values for the shared model system aged at 70°C are displayed in Table 10, where the dielectric results indicate ~ 1.4% water uptake, compared to a value of ~ 2.4% from the gravimetric data, and a scaling factor of ~ 0.61. This implies that the Kirkwood coefficient is ~0.55 at 70°C which is the reverse of the trend observed with Prime20 where the value increased with increasing temperature. The difference

in behaviour is probably a reflection of the difference in the matrix topography between the matrix materials.

Table 10. Water ingress data for the shared system at 70°C.

T_c /°C	Gravimetric % uptake	Equilibrium $\varepsilon'_t - \varepsilon'_0$ values	Estimated % uptake from $\varepsilon'_t - \varepsilon'_0$ value	Kirkwood coefficient
50	2.7	1.23	1.54	0.57
60	2.2	1.17	1.46	0.66
70	2.2	1.05	1.31	0.60

9.6.1 Conclusions

The dielectric studies indicate the type of water and its distribution whereas the gravimetric data indicates how much moisture is absorbed. Differences in the gravimetric and dielectric responses, with increasing water ingress, reflect the matrix structure where the shared model system is more crosslinked. Using a combination of the two measurement methods it is possible to obtain a greater insight into the nature of the moisture uptake than using either alone.

9.7 REFERENCES

1. Cakmak, M., J.L. White, and J.E. Spruiell, *Structural Characterization Of Crystallinity And Crystalline Orientation In Simultaneously Biaxially Stretched And Annealed Polyethylene Terephthalate Films.* Journal Of Polymer Engineering, 1986. **6**(1-4): p. 291-312.

2. Lee, K. and C. Sung, *Effect of biaxial drawing conditions on orientation and structure of poly(ethylene terephthalate).* Macromolecules, 1993. **26**(13): p. 3289-3294.

3. Liggat, J. and I. Hunter. *Thermal analysis as a tool for manufacturing R&D*. in *Mettler-Toledo Thermal Analysis User Day*. August 2008. Stirling, Scotland.

4. Kirkwood, J., *The Dielectric Polarization of Polar Liquids.* Journal Of Chemical Physics, 1939. **7**: p. 911-919.